

Biomolecular Engineering of Gas Vesicles with Thiol Functionality

Thesis by
Erik Schruck

In Partial Fulfillment of the Requirements for
the Degree of
Doctor of Philosophy in Chemical
Engineering

The Caltech logo, featuring the word "Caltech" in a bold, orange, sans-serif font, centered within a light orange rectangular background.

CALIFORNIA INSTITUTE OF TECHNOLOGY
Pasadena, California

2025
(Defended April 8, 2025)

© 2025

Erik Schrunk

ORCID: 0009-0003-2002-7411

ACKNOWLEDGEMENTS

The very fact that I am in this position right now—finishing up my PhD at Caltech, writing my doctoral thesis, reflecting happily on the last six-odd years—is a testament to the support, patience, friendship, mentorship, and love of so many people (and two cats).

First off, I would like to thank my advisor, Mikhail Shapiro, for his guidance and encouragement over my time at Caltech. Throughout our many, many 1:1s and interactions over the years, Mikhail has always been thoughtful, inspiring, and kind. He is patient and understanding, but also firmly and diplomatically straightforward when he needs to be; he bears my goals in mind whenever we talk; and he is exceptionally generous with his time, resources, and ideas. None of this would be possible without him. Thanks again, Mikhail!

Second, I would like to thank my thesis committee members: David Tirrell, Kaihang Wang, and Linda Hsieh-Wilson. All three kindly offered constructive, thoughtful feedback on my candidacy report which, looking back, did not deserve such polite treatment (here's hoping this one is a little better!). They all took time to accommodate me and my needs in the months leading up to the completion of this thesis, even despite my rushed planning and their incredibly busy schedules. And, naturally, I chose them for my committee because I look up to each of them as outstanding scientists and role models.

I also want to thank members of the Shapiro Lab. Di mentored me and met with me individually on a regular basis, which was especially important these last few months while Mikhail was in France. I certainly could not have done any of this without his help. George, my rotation mentor, extended to me the same patience and understanding as Mikhail during my rotation, and taught me so much despite being busy with more important things. The lab management team—especially Rosie, Dina, and Margaret—has also done an amazing job keeping things operational in a very full lab of people who work weekends, late nights, and everything in between. I would also like to thank Ishaan, my one and only rotation student, who probably ended up mentoring me more than the other way around; Rob, who helped me so much early on in setting up my mutant library; Przemek, whose work in solving the structure of GvpA made my life so much easier; Sunho, whose ultrasound patterns blew my

mind; Jee Won, Pierina, and George, whom I could always count on for a boba run; Bill and Yuxing, whom I could go to with chemistry questions; our collaborator Reid, whose mixture of goofiness and seriousness made him so fun to have around; and really just everyone in the entire lab.

While I see my lab mates virtually every day, I also could not imagine my time here without my friends from other labs. I'd specifically like to thank Mark for his passion for softball, Vignesh and Siddharth for all the hours we've spent playing squash together, Bobby for all our philosophical discussions, and everyone on all the many softball teams that I've played on during my time here.

I am incredibly grateful for my friends outside of Caltech as well. I'd like to give a huge shoutout to my high school friends: Boss, Mike, Rory, Mark, Jono, Liam, and the rest of the Brofarm—they've both helped me through very low times and been with me for some of the happiest adventures of my whole life. Whether they know it or not, they inspire me to think big, be silly, appreciate beauty, challenge myself, and love others—the exact things I need to do when I bury my head too deep into my problems and forget to look up. And to my college friends, Thoasin, Rajat, Adi, and Erik: through their companionship, help with problem sets, late night food runs, and overall good vibes, they got me through college, and still support me to this day. I also want to acknowledge all my housemates over the years, especially Kelly, Teo, Alex, and Claire, who welcomed me into their home, tolerated my topsy-turvy schedule, and have been such a joy to hang out with.

As if GVs weren't featured enough in this thesis, I'd also like to thank my mentor George V, who reminds me to trust myself and follow my soul.

I thank my undergraduate PI, Robert Farrauto, and research mentor, Ashley Wang, for helping me get started with research. Although my research in the Shapiro Lab is completely different from what I was doing back in New York, it was my very positive experience in the Farrauto Lab that inspired me to go for a doctoral degree.

My family has always been an enormous part of my life, even after I left to go to college on the East Coast. Being back in California with them close by has truly been a blessing. I imagine it is virtually impossible for a parent to know when to be the bad guy and offer harsh, often unwanted life lessons versus when to silently look on as their adult child fumbles through things and learns those lessons for themselves, yet it really feels like my mom and dad managed to toe that line magnificently over the years. Sure, there have been disagreements here and there, but at the end of the day, I feel supported and loved. I know they are proud of me, and I am proud to be their son. I also thank my sister Brigitte, one of my most trusted confidants, who never stops caring for me, listening to my problems, and making me food. The fact that we will always be close—from playing with our stuffed animals as kids to being best friends as adults—is something that I will never take for granted, although I cannot fully rule out the possibility that she only visits me to see my cats.

Speaking of which, I must also acknowledge my two cats, Pamplemousse and Peach-Pear. While everyone else in this entire section contributed positively in some way to the completion of my thesis, this pair of outlaws did the opposite—if not for them, I could have done more research, graduated sooner, spent more time at the gym, and gotten better quality sleep. But I could not be happier that they are part of my life. If being woken up by Pamplemousse asking for cuddles or being harassed by Pear-Pear begging to play fetch continues to impact my productivity in the future, so help me, I will happily suffer the consequences.

I have been welcomed, cared for, and honestly a little spoiled by the family of my girlfriend. I graciously thank Hua, Jenny, Ming, and Mike not only for their generosity (in sharing food, furniture, their time, their homes, and more with me) but also for their guidance. Whether they know it or not, they have mentored me and provided me with amazing role models—both individually and as a whole family—that I wish to emulate. I look up to each of them so much and am deeply honored to have received their acceptance and trust.

Lastly, I must thank my partner, Ann, who supports and inspires me on so many different levels. I admire her intelligence, thoughtfulness, resourcefulness, and goofiness, which

manifest in the way she brightens not just my day, but that of everyone around her. We share a deep understanding, and that feeling of being understood by someone so special to me energizes me in a way no lab result, hobby, or other person can. I am eternally grateful for her, and I thank whatever forces or favorable circumstances brought her into my life. I have a whole bunch more cheesy things to say about her, but I will have plenty of opportunities to tell them to her in person during the rest of our lives together.

To recap, I want to thank a ton of people for all the ways they have helped me on this journey. Now let's talk about some GVs.

ABSTRACT

Therapies involving the administration of engineered cells, such as CAR-T cell therapy and the delivery of genetically modified gut microbes, have enjoyed clinical success and increasing interest in recent years. While these therapies continue to show great promise, the opacity of tissue precludes the use of light in the observation and potential manipulation of these engineered cells as they carry out their functions within the body. To access these cells non-invasively in deep tissue requires the use of imaging modalities that do not involve light, of which ultrasound (US) is especially appealing due to its relatively low cost, safety, and widespread availability. Engineered cells can exhibit US contrast by expressing gas vesicles (GVs), air-filled polymeric proteinaceous nanostructures; GVs have already been used as acoustic reporters for gut colonization, tumor cell activity, and more.

Whereas GVs are most notable for their acoustic properties, we set out to further expand the function of GVs by chemically modifying them at the genetic level. Our goals were twofold: we wished to equip the external, solution-facing side of GVs with a unique chemical handle; and we wished to hide a reactive group within the internal, air-facing side of GVs that could only be revealed when the GV structures are irreversibly collapsed. To accomplish both these goals, we chose to incorporate cysteine into the shell of GVs because cysteine's thiol side chain is chemically unique among all natural amino acids and because wild-type GVs do not contain cysteine in their shells. We set up a cysteine scanning mutant library of the GV shell protein, GvpA/GvpA1, and screened for cysteine-tolerant mutations in the gene. Through this process, we discovered cysteine substitutions that furnished thiol groups facing both the GV exterior and interior.

The GV-exterior-facing cysteines were leveraged to develop a modified GvpA that contains the bioorthogonal six amino acid tetracysteine tag, or TC tag. The TC tag reacts with the membrane-permeable molecule FIAsh, which becomes fluorescent upon reaction. We used TC-tagged GvpA, or tcGvpA, to express GVs in HEK 293T cells, and used confocal microscopy of FIAsh to study those GVs. Notably, we only substituted a small percentage of GvpA to tcGvpA, leaving the rest of the GvpA as wild type; to our knowledge, this is the

only report of a polymeric proteinaceous structure that employs this chimeric assembly approach being successfully expressed and labeled with FIAsh. The microscopy results from this study were used to generate three-dimensional renderings that provided insights into the size and positioning of GV clusters expressed within HEK 293T cells.

Second, we identified several interior-facing cysteine mutants to the GV shell protein GvpA1, which we used to develop “SonoCages”: chemical entities whose reactivity is gated by US. We purified GVs with one mutation from our screen, V47C, and reacted them with monobromobimane (mBBr), a fluorogenic, thiol-reactive molecule. The mutant GVs only reacted with mBBr after treatment with US, which collapsed the GVs and exposed their hydrophobic interiors to the bulk solution. Thus, we had developed thiol-bearing SonoCages whose cysteines could only engage in reactions after US-mediated collapse of the GVs—a process we call “sono-uncaging” in analogy to photo-uncaging. We further demonstrated the utility of SonoCages by preparing a hydrogel containing SonoCages and mBBr and using US to create fluorescent patterns corresponding to regions of GV collapse.

The work presented in this thesis not only demonstrates the functionalization of the GV interior and exterior, but also establishes a framework through which further modifications can be performed. Whereas we used cysteine as our reactive chemical of choice, other amino acids (including non-canonical amino acids) could be used to explore a much wider library of reactivities. The vast potential of GV chemical modification, along with the amazing results from the rest of the Shapiro Lab and in labs across the world, serves as a reminder that GVs and GV-based technologies are not just a bubble (pun intended)—they are going to be around for a long time.

PUBLISHED CONTENT AND CONTRIBUTIONS

Schrunk, E.; Dutka, P.; Hurt, R. C.; Wu, D.; Shapiro, M. G. Bioorthogonal Labeling Enables In Situ Fluorescence Imaging of Expressed Gas Vesicle Nanostructures. *Bioconjug. Chem.* **2024**, 35 (3), 333–339. <https://doi.org/10.1021/acs.bioconjchem.3c00518>.

ES conceived the study, conducted experiments, performed microscopy and image analysis, and wrote the manuscript.

Schrunk, E.; Lee, S.; Dutka, P.; Wu, D.; Shapiro, M. G. Sono-Uncaging of Engineered Gas Vesicles for Spatiotemporal Control of Thiol Reactivity. *Manuscript in preparation*.

ES conceived the study, conducted experiments with DW and SL, performed microscopy and image analysis, and prepared the manuscript.

TABLE OF CONTENTS

Acknowledgements	iii
Abstract.....	vii
Published Content and Contributions	ix
Table of Contents	x
List of Figures	xi
Nomenclature and Abbreviations	xii
Chapter 1: Introduction and motivation.....	1
1.1 Invasiveness of optical methods in molecular biology	1
1.2 Ultrasound and gas vesicles	2
1.3 This work: chemical functionalization of GVs with cysteine.....	3
1.4 References	4
Chapter 2: Bioorthogonal labeling enables in situ fluorescence imaging of expressed gas vesicle nanostructures.....	8
2.1 Abstract	8
2.2 Introduction	9
2.3 Results and discussion	10
2.4 Conclusion	17
2.5 Experimental methods	17
2.6 Acknowledgements.....	20
2.7 References	20
2.8 Supporting information.....	23
Chapter 3: Sono-uncaging of engineered gas vesicles for spatiotemporal control of thiol reactivity.....	28
3.1 Abstract	28
3.2 Introduction	29
3.3 Results and discussion	31
3.4 Conclusion	35
3.5 Experimental methods	36
3.6 References	42
3.7 Supporting information.....	46
Chapter 4: Conclusion, future directions, and final thoughts.....	49
4.1 Incorporation of non-canonical amino acids into GVs	49
4.2 GVs with exterior disulfide bonds and multiple mutations to GvpA1	50
4.3 Expressing chimeric GVs in HEK 293T cells with a WT/modified GvpA cocktail	51
4.4 Final thoughts.....	51
4.5 References	51
All references	54

LIST OF FIGURES

Figure and description	Pages
Figure 2.1: The C-terminus of the gas vesicle structural protein GvpA is tolerant of point mutations to cysteine.	11
Figure 2.2: The C-terminus of GvpA tolerates substitution to the tetracysteine motifs CC--CC and CCPGCC.	13
Figure 2.3: tcGVs can be successfully expressed and labeled with FLAsH in HEK 293T cells.	14
Figure 2.4: Fluorescence imaging of tcGVs elucidates the size and spatial distributions of GV clusters in HEK 293T cells.	16
Figure 2.S1: Sequence alignment for <i>Anabaena flos-aquae</i> gvpA and <i>Serratia</i> sp. 39006 gvpA1.	23
Figure 2.S2: Opacity screen of mutant gvpA1 plasmids in <i>E. coli</i> .	24
Figure 2.S3: Images of FLAsH-labeled GV in cells transfected with different ratios of wtGvpA:tcGvpA.	25
Figure 2.S4: 3D renderings of tcGV-expressing cells.	26
Figure 3.1: Sono-uncaging and SonoCages.	30
Figure 3.2: GvpA1 cysteine scanning library identifies several SonoCage candidates with potentially inward-facing cysteine side chains.	32
Figure 3.3: SonoCages (V47C mutant GV) undergo sono-uncaging of cysteine in solution and in agarose hydrogels.	33-34
Figure 3.4: Sono-uncaging of SonoCages leads to patterning of thiol reactivity with spatiotemporal control in an agarose gel.	35
Figure 3.S1: Sequence alignment for <i>Anabaena flos-aquae</i> gvpA and <i>Serratia</i> sp. 39006 gvpA1.	46
Figure 3.S2: SonoCage candidate screen on patch plates.	47
Figure 3.S3: Confocal microscopy images of mBBr fluorescence in WT GV and SonoCage samples prepared in PBS on a glass-bottomed dish.	48

NOMENCLATURE AND ABBREVIATIONS

GV: Gas vesicle; an air-filled, proteinaceous nanostructure.

US: Ultrasound; high-frequency sound waves that form the basis of ultrasound imaging, a non-invasive imaging modality.

FIAsH: Fluorescein Arsenical Hairpin Binder; a membrane-permeable, green fluorogenic molecule activated by binding to the tetracysteine tag.

TC (tag): Tetracysteine tag; a motif of six consecutive amino acids with the pattern CCXYCC, where C is cysteine and X and Y are any other amino acids. The optimized TC tag is CCPGCC, where P is proline and G is glycine.

mBBr: Monobromobimane; a fluorogenic molecule that reacts with reduced thiols.

ncAA: Non-canonical amino acid; a proteinogenic amino acid that is not found in nature.

INTRODUCTION AND MOTIVATION

1.1 Invasiveness of optical methods in molecular biology

The interaction of biomolecules with light underpins molecular biology research to an undeniable extent. Fluorescent proteins alone have revolutionized the fields of biology and biological engineering;¹ other optical methods such as optogenetics,^{2,3} photo-uncaging,⁴⁻⁷ and more have similarly enabled countless breakthroughs. Yet arguably the greatest single aim of the field of biology—the betterment of human health—poses a challenge wherein many of the optics-based techniques in the molecular biology toolbox are ineffectual: human tissue itself, in which visible light is mostly scattered and absorbed past a depth of 1 mm.⁸ And while therapies that act within deep tissue such as adoptive cell therapy^{9,10} and use of engineered gut microbes^{11,12} have made enormous strides within the last several decades despite the obstacle of tissue opacity, the ability to “see” or even “talk to” those therapeutic agents *in vivo* would constitute a key advance in the understanding and further development of those technologies.

Optical methods have been used to study processes in tissue, albeit with significant limitations. For example, histology and fluorescence-activated cell sorting can be used to make sense of biological samples extracted from test subjects (usually via a biopsy or following sacrifice of the animal, which both constitute invasive procedures), but lack *in vivo* context. In the cases of shallow^{13,14} or transparent¹⁵⁻¹⁷ tissue, light-emitting proteins like fluorescent proteins or luciferases can serve as reporters *in vivo*. However, light-based imaging of deep tissue predominantly involves invasive procedures. Intravital microscopy is performed on live animals but usually requires the surgical construction of an imaging window to access deep tissue in opaque organisms.¹⁸ Techniques like multi-photon intravital microscopy push the limits of tissue penetration by using relatively low-frequency light

(which increases penetration depth), but this imaging depth is still on the order of a millimeter.^{19,20} Thus, despite the abundance and convenience of optical methods, light cannot be used to study processes in deep tissue without some degree of invasiveness.

1.2 Ultrasound and gas vesicles

Imaging modalities that rely on forms of energy other than light such as ultrasound (US) imaging, magnetic resonance imaging (MRI), and positron emission tomography (PET) feature much greater penetration depth into tissue than light⁸ and thus represent non-invasive means of accessing data from deep within the body. Of these, US is particularly appealing due to its penetration depth (~1-100 cm), resolution (~100 μm), ease and low cost of use, and lack of ionizing radiation.^{21,22} However, whereas optical imaging enjoys a sophisticated toolbox of light-interactive genetically encodable elements like fluorescent proteins and channelrhodopsins, US has traditionally lacked analogous genes.

That has begun to change in recent years. The young field of sonogenetics couples US-derived forces with mechanosensitive ion channels to control cellular activity, in likeness to optogenetics.^{22,23} And the US counterparts of fluorescent proteins, genetically encodable acoustic reporter proteins, have also recently entered use in the biomedical field.

These “US counterparts of fluorescent proteins” are, of course, gas vesicles (GVs). GV are nanoscale (~100 nm diameter, ~500 nm length²⁴) cylindrical proteinaceous air-filled structures natively found in certain species of microorganisms and have been known and studied for over a century.²⁵ They naturally feature air-water interfaces, providing them with high US contrast due to the large compressibility and density differences between air and water. The genes encoding GV expression were recently moved into bacteria²⁶ and mammalian cells,^{21,27} establishing GV as genetically encodable US contrast agents. GV have served as US-based reporters of cellular function,²⁸ ultrasonic cavitation nuclei,²⁹ actuators for cellular manipulation via US,³⁰ and more.

When I came to Caltech in 2018, I rotated in the Shapiro Lab and was sold on the utility and beauty of GVs. And, as if the novelty of the situation—of being at a new school, of doing biological research for the first time, of learning about US for the first time—was not enough, I decided somewhat naively that I wanted to further add to the function of GVs by modifying them chemically.

1.3 This work: chemical functionalization of GVs with cysteine

Whenever I explain my PhD work to someone, I start by describing GVs. The question I almost always get asked during the process is, “cool—can you put something inside of them?” That too was my question when I began my rotation with the Shapiro Lab.

The air-filled interior of GVs is, unsurprisingly, extremely hydrophobic. The small (~7.4 kDa) structural protein GvpA/GvpA1, which makes up the GV shell, is one of the most hydrophobic proteins known.^{25,31} To load a peptide or enzyme into the GV would presumably subject it to misfolding due to the severe conditions on the GV interior. Also, as the exact mechanism of GV assembly is not known, the best approach for introducing an external element into the GV is likely by attachment of that element to GvpA, but the highly conserved nature²⁴ and small size of GvpA all but precludes fusions to the protein. Given these conditions, I hypothesized that the most feasible way to load something into the GV was to incorporate a reactive amino acid in the GV-interior-facing region of GvpA.

As I will discuss in Chapter 3, I chose to use cysteine as the reactive amino acid mentioned above due to its unique reactivity among natural amino acids and its absence from wild-type GvpA. With a lot of help from the lab, I set up a cysteine scanning mutant library of GvpA/GvpA1 to help identify cysteine-tolerant amino acid sites. It was through that mutant library that I explored the incorporation of cysteine into the GV shell, endowing the GV with the thiol functional group. In this thesis, I will discuss the two main results of this exploration: the introduction of the tetracysteine tag into the GV exterior, which we used to study the locations of newly expressed GV clusters within mammalian cells; and the concealment of a

single cysteine's thiol side chain within the GV interior, which served as a source of reactive reduced thiol only once the GVs were irreversibly collapsed with US.

1.4 References

- (1) Tsien, R. Y. The Green Fluorescent Protein. *Annu. Rev. Biochem.* **1998**, *67* (1), 509–544. <https://doi.org/10.1146/annurev.biochem.67.1.509>.
- (2) Deisseroth, K. Optogenetics: 10 Years of Microbial Opsins in Neuroscience. *Nat. Neurosci.* **2015**, *18* (9), 1213–1225. <https://doi.org/10.1038/nn.4091>.
- (3) Pan, Z.-H.; Lu, Q.; Bi, A.; Dizhoor, A. M.; Abrams, G. W. Optogenetic Approaches to Restoring Vision. *Annu. Rev. Vis. Sci.* **2015**, *1* (1), 185–210. <https://doi.org/10.1146/annurev-vision-082114-035532>.
- (4) Ellis-Davies, G. C. R. Caged Compounds: Photorelease Technology for Control of Cellular Chemistry and Physiology. *Nat. Methods* **2007**, *4* (8), 619–628. <https://doi.org/10.1038/nmeth1072>.
- (5) Adams, S. R.; Kao, J. P. Y.; Grynkiewicz, G.; Minta, A.; Tsien, R. Y. Biologically Useful Chelators That Release Ca²⁺ upon Illumination. *J. Am. Chem. Soc.* **1988**, *110* (10), 3212–3220. <https://doi.org/10.1021/ja00218a034>.
- (6) Klöcker, N.; Weissenboeck, F. P.; Van Dülmen, M.; Špaček, P.; Hüwel, S.; Rentmeister, A. Photocaged 5' Cap Analogues for Optical Control of mRNA Translation in Cells. *Nat. Chem.* **2022**, *14* (8), 905–913. <https://doi.org/10.1038/s41557-022-00972-7>.
- (7) Kaplan, J. H.; Forbush, B.; Hoffman, J. F. Rapid Photolytic Release of Adenosine 5'-Triphosphate from a Protected Analog: Utilization by the Sodium:Potassium Pump of Human Red Blood Cell Ghosts. *Biochemistry* **1978**, *17* (10), 1929–1935. <https://doi.org/10.1021/bi00603a020>.
- (8) Piraner, D. I.; Farhadi, A.; Davis, H. C.; Wu, D.; Maresca, D.; Szablowski, J. O.; Shapiro, M. G. Going Deeper: Biomolecular Tools for Acoustic and Magnetic Imaging and Control of Cellular Function. *Biochemistry* **2017**, *56* (39), 5202–5209. <https://doi.org/10.1021/acs.biochem.7b00443>.

- (9) Rosenberg, S. A.; Restifo, N. P.; Yang, J. C.; Morgan, R. A.; Dudley, M. E. Adoptive Cell Transfer: A Clinical Path to Effective Cancer Immunotherapy. *Nat. Rev. Cancer* **2008**, *8* (4), 299–308. <https://doi.org/10.1038/nrc2355>.
- (10) Sterner, R. C.; Sterner, R. M. CAR-T Cell Therapy: Current Limitations and Potential Strategies. *Blood Cancer J.* **2021**, *11* (4), 69. <https://doi.org/10.1038/s41408-021-00459-7>.
- (11) Riglar, D. T.; Silver, P. A. Engineering Bacteria for Diagnostic and Therapeutic Applications. *Nat. Rev. Microbiol.* **2018**, *16* (4), 214–225. <https://doi.org/10.1038/nrmicro.2017.172>.
- (12) Charbonneau, M. R.; Isabella, V. M.; Li, N.; Kurtz, C. B. Developing a New Class of Engineered Live Bacterial Therapeutics to Treat Human Diseases. *Nat. Commun.* **2020**, *11* (1), 1738. <https://doi.org/10.1038/s41467-020-15508-1>.
- (13) Luker, K. E.; Luker, G. D. Bioluminescence Imaging of Reporter Mice for Studies of Infection and Inflammation. *Antiviral Res.* **2010**, *86* (1), 93–100. <https://doi.org/10.1016/j.antiviral.2010.02.002>.
- (14) Liu, S.; Su, Y.; Lin, M. Z.; Ronald, J. A. Brightening up Biology: Advances in Luciferase Systems for in Vivo Imaging. *ACS Chem. Biol.* **2021**, *16* (12), 2707–2718. <https://doi.org/10.1021/acscchembio.1c00549>.
- (15) Benard, E. L.; Van Der Sar, A. M.; Ellett, F.; Lieschke, G. J.; Spaink, H. P.; Meijer, A. H. Infection of Zebrafish Embryos with Intracellular Bacterial Pathogens. *J. Vis. Exp.* **2012**, No. 61, 3781. <https://doi.org/10.3791/3781>.
- (16) Meijer, A. H.; Van Der Vaart, M.; Spaink, H. P. Real-Time Imaging and Genetic Dissection of Host-Microbe Interactions in Zebrafish: Dissecting Host-Microbe Interactions in Zebrafish. *Cell. Microbiol.* **2014**, *16* (1), 39–49. <https://doi.org/10.1111/cmi.12236>.
- (17) Levraud, J.-P.; Palha, N.; Langevin, C.; Boudinot, P. Through the Looking Glass: Witnessing Host–Virus Interplay in Zebrafish. *Trends Microbiol.* **2014**, *22* (9), 490–497. <https://doi.org/10.1016/j.tim.2014.04.014>.

- (18) Secklehner, J.; Lo Celso, C.; Carlin, L. M. Intravital Microscopy in Historic and Contemporary Immunology. *Immunol. Cell Biol.* **2017**, *95* (6), 506–513. <https://doi.org/10.1038/icb.2017.25>.
- (19) Choe, K.; Hontani, Y.; Wang, T.; Hebert, E.; Ouzounov, D. G.; Lai, K.; Singh, A.; Béguelin, W.; Melnick, A. M.; Xu, C. Intravital Three-Photon Microscopy Allows Visualization over the Entire Depth of Mouse Lymph Nodes. *Nat. Immunol.* **2022**, *23* (2), 330–340. <https://doi.org/10.1038/s41590-021-01101-1>.
- (20) Ouzounov, D. G.; Wang, T.; Wang, M.; Feng, D. D.; Horton, N. G.; Cruz-Hernández, J. C.; Cheng, Y.-T.; Reimer, J.; Tolia, A. S.; Nishimura, N.; Xu, C. In Vivo Three-Photon Imaging of Activity of GCaMP6-Labeled Neurons Deep in Intact Mouse Brain. *Nat. Methods* **2017**, *14* (4), 388–390. <https://doi.org/10.1038/nmeth.4183>.
- (21) Farhadi, A.; Ho, G. H.; Sawyer, D. P.; Bourdeau, R. W.; Shapiro, M. G. Ultrasound Imaging of Gene Expression in Mammalian Cells. *Science* **2019**, *365* (6460), 1469–1475. <https://doi.org/10.1126/science.aax4804>.
- (22) Maresca, D.; Lakshmanan, A.; Abedi, M.; Bar-Zion, A.; Farhadi, A.; Lu, G. J.; Szablowski, J. O.; Wu, D.; Yoo, S.; Shapiro, M. G. Biomolecular Ultrasound and Sonogenetics. *Annu. Rev. Chem. Biomol. Eng.* **2018**, *9* (1), 229–252. <https://doi.org/10.1146/annurev-chembioeng-060817-084034>.
- (23) Ibsen, S.; Tong, A.; Schutt, C.; Esener, S.; Chalasani, S. H. Sonogenetics Is a Non-Invasive Approach to Activating Neurons in *Caenorhabditis Elegans*. *Nat. Commun.* **2015**, *6* (1), 8264. <https://doi.org/10.1038/ncomms9264>.
- (24) Dutka, P.; Metskas, L. A.; Hurt, R. C.; Salahshoor, H.; Wang, T.-Y.; Malounda, D.; Lu, G. J.; Chou, T.-F.; Shapiro, M. G.; Jensen, G. J. Structure of *Anabaena Flos-Aquae* Gas Vesicles Revealed by Cryo-ET. *Structure* **2023**, *31* (5), 518-528.e6. <https://doi.org/10.1016/j.str.2023.03.011>.
- (25) Walsby, A. E. Gas Vesicles. *Microbiol. Rev.* **1994**, *58* (1), 94–144. <https://doi.org/10.1128/mr.58.1.94-144.1994>.
- (26) Bourdeau, R. W.; Lee-Gosselin, A.; Lakshmanan, A.; Farhadi, A.; Kumar, S. R.; Nety, S. P.; Shapiro, M. G. Acoustic Reporter Genes for Noninvasive Imaging of

- Microorganisms in Mammalian Hosts. *Nature* **2018**, *553* (7686), 86–90. <https://doi.org/10.1038/nature25021>.
- (27) Hurt, R. C.; Buss, M. T.; Duan, M.; Wong, K.; You, M. Y.; Sawyer, D. P.; Swift, M. B.; Dutka, P.; Barturen-Larrea, P.; Mittelstein, D. R.; Jin, Z.; Abedi, M. H.; Farhadi, A.; Deshpande, R.; Shapiro, M. G. Genomically Mined Acoustic Reporter Genes for Real-Time in Vivo Monitoring of Tumors and Tumor-Homing Bacteria. *Nat. Biotechnol.* **2023**, *41* (7), 919–931. <https://doi.org/10.1038/s41587-022-01581-y>.
- (28) Lakshmanan, A.; Jin, Z.; Nety, S. P.; Sawyer, D. P.; Lee-Gosselin, A.; Malounda, D.; Swift, M. B.; Maresca, D.; Shapiro, M. G. Acoustic Biosensors for Ultrasound Imaging of Enzyme Activity. *Nat. Chem. Biol.* **2020**, *16* (9), 988–996. <https://doi.org/10.1038/s41589-020-0591-0>.
- (29) Bar-Zion, A.; Nourmahnad, A.; Mittelstein, D. R.; Shivaiei, S.; Yoo, S.; Buss, M. T.; Hurt, R. C.; Malounda, D.; Abedi, M. H.; Lee-Gosselin, A.; Swift, M. B.; Maresca, D.; Shapiro, M. G. Acoustically Triggered Mechanotherapy Using Genetically Encoded Gas Vesicles. *Nat. Nanotechnol.* **2021**, *16* (12), 1403–1412. <https://doi.org/10.1038/s41565-021-00971-8>.
- (30) Wu, D.; Baresch, D.; Cook, C.; Ma, Z.; Duan, M.; Malounda, D.; Maresca, D.; Abundo, M. P.; Lee, J.; Shivaiei, S.; Mittelstein, D. R.; Qiu, T.; Fischer, P.; Shapiro, M. G. Biomolecular Actuators for Genetically Selective Acoustic Manipulation of Cells. *Sci. Adv.* **2023**, *9* (8), eadd9186. <https://doi.org/10.1126/sciadv.add9186>.
- (31) Belenky, M.; Meyers, R.; Herzfeld, J. Subunit Structure of Gas Vesicles: A MALDI-TOF Mass Spectrometry Study. *Biophys. J.* **2004**, *86* (1), 499–505. [https://doi.org/10.1016/S0006-3495\(04\)74128-4](https://doi.org/10.1016/S0006-3495(04)74128-4).

BIOORTHOGONAL LABELING ENABLES IN SITU FLUORESCENCE IMAGING OF EXPRESSED GAS VESICLE STRUCTURES

Schrunk, E.; Dutka, P.; Hurt, R. C.; Wu, D.; Shapiro, M. G. Bioorthogonal Labeling Enables In Situ Fluorescence Imaging of Expressed Gas Vesicle Nanostructures. *Bioconjug. Chem.* **2024**, *35* (3), 333–339. <https://doi.org/10.1021/acs.bioconjchem.3c00518>.

2.1: Abstract

Gas vesicles (GVs) are proteinaceous nanostructures that, along with virus-like particles, encapsulins, nano-cages, and other macromolecular assemblies are being developed for potential biomedical applications. To facilitate such development, it would be valuable to characterize these nanostructures' sub-cellular assembly and localization. However, traditional fluorescent protein fusions are not tolerated by GV's primary constituent protein, making optical microscopy a challenge. Here, we introduce a method for fluorescently visualizing intracellular GV's using the bioorthogonal label FIAsh, which becomes fluorescent upon reacting with the six-amino acid tetracysteine (TC) tag. We engineered the GV subunit protein, GvpA, to display the TC tag, and showed that GV's bearing TC-tagged GvpA can be successfully assembled and fluorescently visualized in HEK 293T cells. Importantly, this was achieved by replacing only a fraction of the GvpA with the tagged version. We used fluorescence images of the tagged GV's to study GV size and distance distributions within these cells. This bioorthogonal and fractional labeling approach will enable research to provide a greater understanding of GV's and could be adapted to similar proteinaceous nanostructures.

2.2: Introduction

Gas vesicles (GVs) are air-filled protein nanostructures (~85 nm diameter, ~500 nm length)²⁴ that are entering use in biomedical applications alongside other proteinaceous macromolecular assemblies such as encapsulins, virus-like particles and nano-cages.^{32–34} In particular, GV^s have recently emerged as promising agents for biomolecular ultrasound: they have been expressed recombinantly in both bacterial and mammalian cells and have been used as cavitation nuclei,²⁹ ultrasonic reporters of cancer,²⁷ acoustic actuators for selective cellular manipulation,³⁰ and more.^{26,28,35,36} These GV-based technologies—and those involving other macromolecular complexes—could benefit from knowledge of these structures' sub-cellular localization, as this knowledge could enable the engineering of systems targeted to specific organelles or cellular compartments. However, there are currently no reported methods to fluorescently label GV^s within cells. In part, this is because the composition of GV^s as assemblies of small, highly conserved subunit proteins makes it difficult for them to accommodate substantial fused functionalities such as fluorescent proteins.

Here, we describe a method to optically visualize GV^s inside cells by genetically modifying the GV shell protein GvpA with the tetracysteine (TC) motif, allowing the GV^s to be fluorescently labeled with the bioorthogonal FAsH reagent for visualization of their sub-cellular localization. FAsH is a membrane-permeant fluorogenic molecule that reacts specifically with the TC tag (Cys-Cys-Pro-Gly-Cys-Cys) and which turns on fluorescence upon reaction.^{37–40} We sought to introduce this tag into the major GV structural protein, GvpA, such that expressed intracellular GV^s would be able to react with FAsH and turn on fluorescence. We screened for TC-containing GvpA mutants in bacteria and, once we identified a suitable variant, expressed TC-tagged GV^s (“tcGV^s”) in HEK 293T cells. Using these tcGV^s, we were able to directly visualize the three-dimensional distribution of GV^s in the cell, observing that they tend to form clusters in the cytosol. Notably, these tcGV^s are produced using a mixture of wild type and modified GvpA genes, where only a fraction of the GvpA subunits is tagged with the TC tag. In addition to enabling the study of GV^s, this

fractional labeling approach could inform similar studies of other genetically encoded protein nanostructures.

2.3: Results and discussion

The C-terminus of GvpA is amenable to single substitutions to cysteine.

To engineer tcGVs, we sought to incorporate the TC motif into the GV shell protein GvpA. We looked to introduce the motif into a region of GvpA which faces the GV exterior—thereby making it accessible to cytosolic FLaSH—and which is tolerant of mutations to cysteine, such that introduction of the TC tag does not abrogate GvpA expression and GV assembly. To predict which region of GvpA would best accommodate the TC tag, we looked to structural models of GvpA.^{24,41} In a random mutagenesis experiment, the C-terminus of GvpA was found to be tolerant of many different point mutations – more so than any other region of the protein – suggesting that this region could be the most amenable to the substitution of the six-amino acid TC tag.¹ Furthermore, the C-terminus of GvpA is on the exterior-facing region of the protein¹ (Figure 2.1a-c). We therefore selected the C-terminus of GvpA as our target location.

Before attempting the substitution of four cysteines into GvpA, we first tested the ability of individual positions within its C-terminus to accommodate single-Cys mutations. We screened mutants in *E. coli* using the bARG_{Ser} construct, which uses GV genes derived from *Serratia* sp. 39006, including the GvpA homolog GvpA16 (~92% similarity to GvpA, sequence alignment in Figure 2.S1). We mutated each of the final eight amino acids in GvpA1 to Cys (Figure 2.1d-e), then expressed the mutant GVs in bacterial patches on Petri dishes containing the inducer arabinose. We then measured the opacity of the patches as a proxy for GV expression, as GVs scatter visible light.⁴²⁻⁴⁴ We observed GV expression in all mutants, with only modest reductions at positions 69-71 (Figure 2.1e), and concluded that the C-terminus of GvpA1 could tolerate point mutations to Cys.

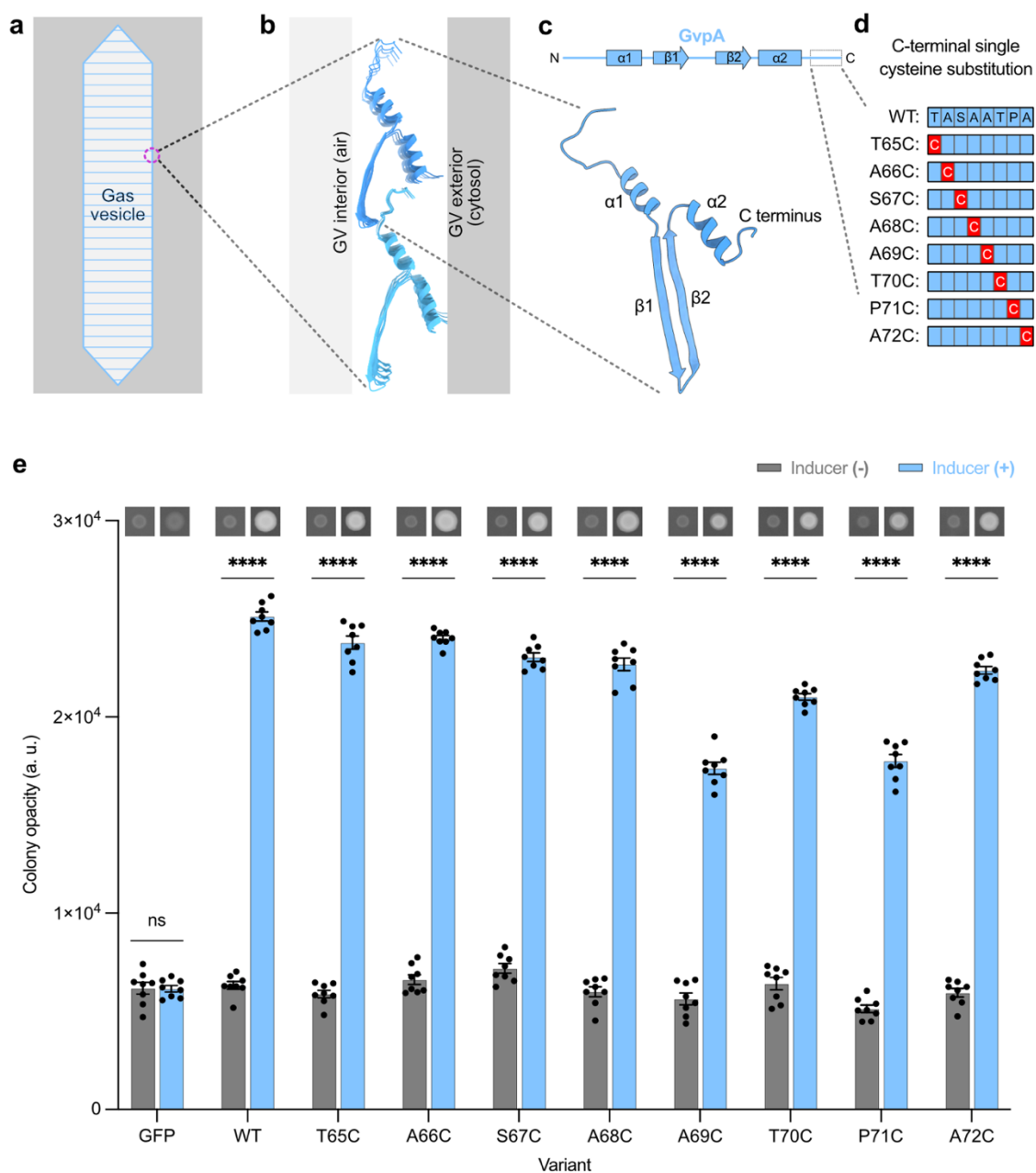


Figure 2.1: The C-terminus of the gas vesicle structural protein GvpA is tolerant of point mutations to cysteine. (a) Illustration of a single gas vesicle. (b) Atomic model of two adjacent “ribs” composed of GvpA (PDB 8GBS)²⁴. Interior- and exterior-facing sides of the GV shell indicated. (c) Linear and atomic models of a single GvpA molecule with alpha helix and beta strand regions indicated. The C-terminal region of GvpA is shown by a dashed box in the linear representation of GvpA. (d) Schematic of the C-terminal variants of GvpA1 screened. Each red box represents a point mutation to cysteine and each blue box represents the amino acid in the wild type GvpA1. (e) Graph of opacity for induced and uninduced bacterial patches transformed with plasmids coding for mutant GV expression. Colony opacity is indicative of GV expression.

The C-terminus of GvpA is amenable to substitutions to the TC tag.

With the knowledge that each amino acid in the C-terminus of GvpA1 could be individually substituted to Cys, we next tested multi-position substitutions to introduce the TC tag. We cloned three variants of the GvpA1 gene with the minimal TC tag (Cys-Cys-Xxx-Yyy-Cys-Cys) in all three possible C-terminal positions (Figure 2.2a), leaving the middle two non-Cys amino acids of the tag unchanged relative to wild type (WT) GvpA1 (denoted by Xxx and Yyy) to minimize sequence disruption. We found GV expression in all cases (Figure 2.2b), although at reduced levels compared to wild type. The variant with the TC tag at the most C-terminal position, called TC3, had the highest opacity (Figure 2.2b) and the healthiest patch morphology (Figure 2.S2), suggesting that this variant was the best tolerated by cells expressing the resulting GVs. As an additional test, we converted the two non-Cys residues in TC3 to Pro-Gly to create a full TC tag (Cys-Cys-Pro-Gly-Cys-Cys) (Figure 2.2a) and noted that this mutant, called TC4, expressed GVs as well (Figure 2.2b). We concluded that the optimal positioning of the TC tag in the C-terminus of GvpA1 was at the most C-terminal position.

Tetracysteine-tagged GvpA can be incorporated into GVs expressed in mammalian cells and imaged fluorescently by FAsH.

After establishing tcGV expression in bacteria, we set out to translate our approach to mammalian cells. We inserted the TC tag into the GvpA of the mARG construct²⁷ at the same location as the best-performing tetracysteine-tagged GvpA1 from our bacterial screen (TC3) and called the resulting gene “tcGvpA.” We transfected human HEK 293T cells with mARG, replacing 10%, 20%, 25%, and 100% of the wild type GvpA (“wtGvpA”) plasmid with the tcGvpA plasmid in the transfection mixture (molar ratio), and observed GV formation in all but the 100% tcGvpA condition (Figure 2.3b, Figure 2.S3). This shows that while some wtGvpA is necessary for GV formation, tcGvpA expression is well-tolerated by mammalian cells. To determine whether tcGvpA is incorporated into the GVs, we next treated the transfected cells with FAsH and found that FAsH readily labeled the GVs in those cells (Figure 2.3b). Control cells expressing wild type GVs (“wtGVs”) without tcGvpA

did not show labeling (Figure 2.3b). This demonstrated that tcGvpA is incorporated into mammalian GVs when co-expressed with wtGvpA and that the resulting chimeric tcGVs can be labeled intracellularly by FIAsh. tcGVs expressed in cells transfected with 10% and 25% tcGvpA could be labeled with FIAsh (Figure 2.S3) similarly to those with 20% tcGvpA (Figure 2.3b), suggesting that FIAsh labeling does not require a very precise ratio of tcGvpA and wtGvpA.

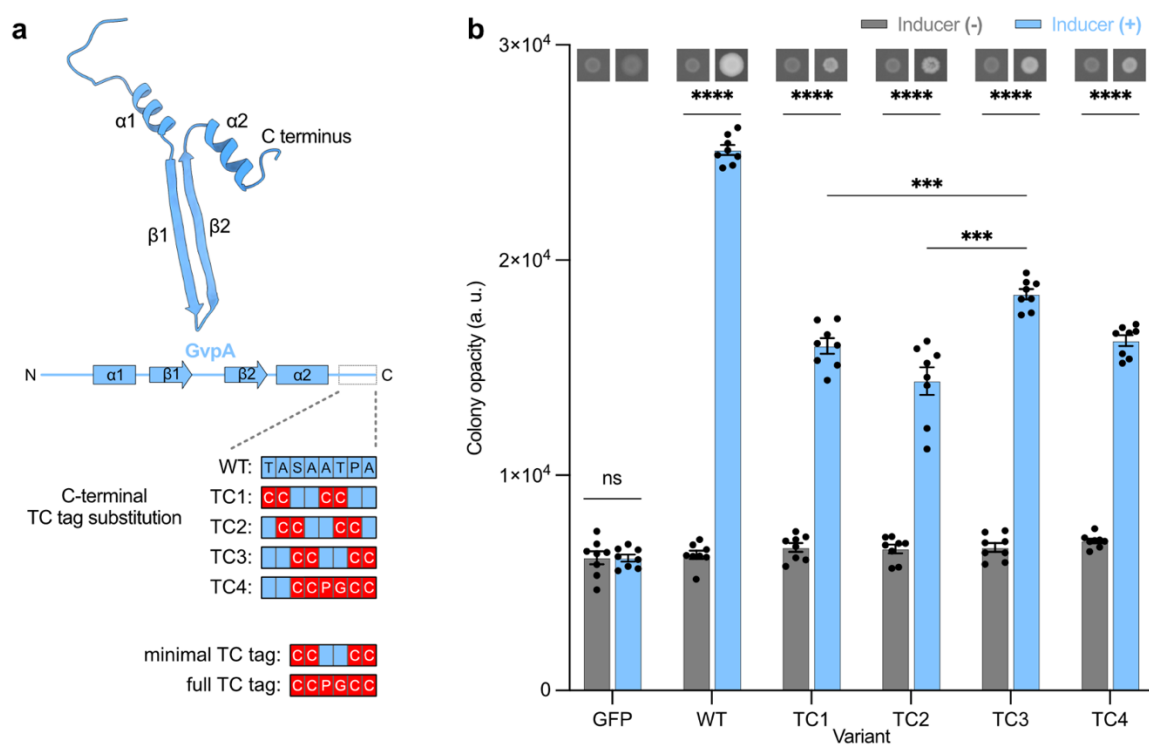


Figure 2.2: The C-terminus of GvpA tolerates substitution to the tetracysteine motifs CC--CC and CCPGCC. (a) Schematic of the C-terminal tetracysteine mutants of GvpA1 screened. Each red “C” box represents a point mutation to cysteine and each blue box represents the amino acid in wild type GvpA1. TC1 through TC3 are the minimal TC tag Cys-Cys-Xxx-Yyy-Cys-Cys, while TC4 is the full TC tag Cys-Cys-Cys-Pro-Gly-Cys-Cys. (b) Graph of opacity for induced and uninduced bacterial patches transformed with plasmids coding for mutant GV expression. Colony opacity is indicative of GV expression. Representative images of induced and uninduced patches displayed above their corresponding columns in the graph. N = 8 patches per condition. Patches with a plasmid encoding GFP expression included as a GV-negative control. Asterisks represent statistical significance by unpaired t-tests (****: $p < 0.0001$, ***: $p < 0.001$, ns: not significant). Error bars represent mean \pm SEM.

The co-delivery of tcGvpA and wtGvpA for tcGV expression is an important aspect of these findings, as it demonstrates that not every protein subunit of the GVs needs to be TC-tagged for the GV itself to be sufficiently reactive towards FIAsh. Therefore, the use of a mixture of wtGvpA and tcGvpA—notably with a significant majority of the wtGvpA gene—to express tcGVs highlights the utility of this approach when attempting to fluorescently label proteinaceous nanostructures within cells: even if TC-tagging a protein subunit is not ideal, spiking in a small fraction of TC-tagged subunits can be sufficient for informative labeling.

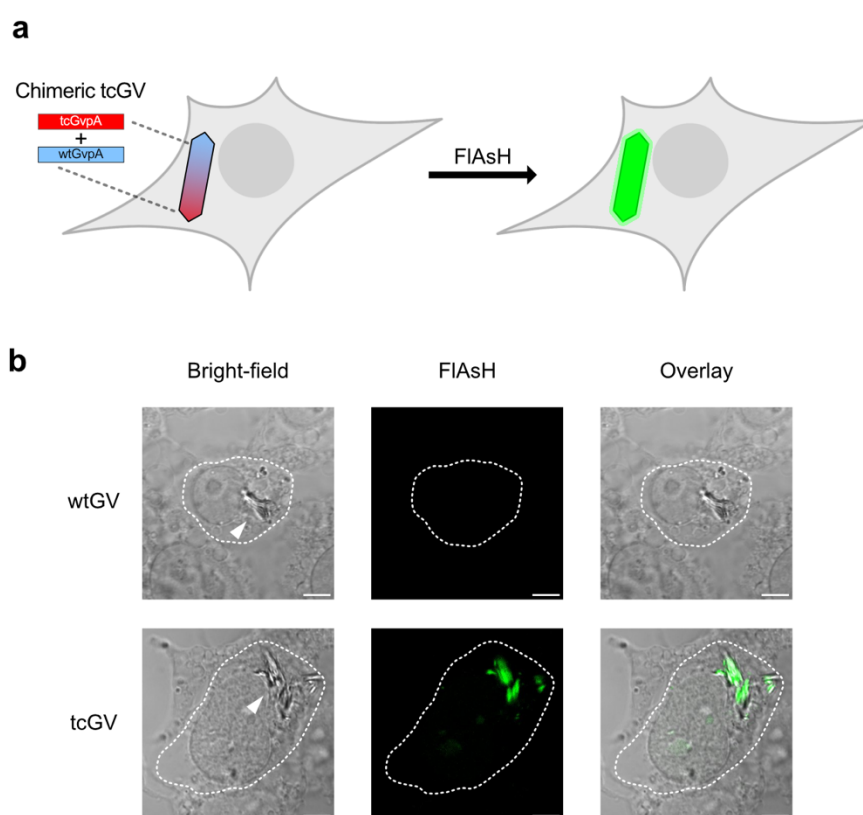


Figure 2.3: tcGVs can be successfully expressed and labeled with FIAsh in HEK 293T cells. (a) Schematic of an expressed tcGV cluster becoming fluorescent with FIAsh. tcGVs are comprised of wtGvpA and tcGvpA. After addition of FIAsh, the tcGVs become fluorescent as FIAsh reacts with tcGvpA. (b) Images of wtGV and tcGV (20% tcGvpA) clusters in fixed HEK 293T cells (indicated by arrows). All GVs are visible under bright-field imaging (first column), but only tcGVs have any FIAsh signal above the background (second column). The bright-field/FIAsh overlay (third column) demonstrates that the strongest FIAsh signal overlaps with tcGV clusters. All scale bars 5 μ m. GV-expressing cells outlined in white.

In addition, the multimeric nature of GVs contributes to their high contrast labeling with FAsH, which may require the concentration of the tagged protein to be higher than several μM to overcome background fluorescence.³⁸ We estimate that the concentration of GvpA within a typical imaging voxel containing one GV is on the order of 300 μM (Section 2.8 Supplemental Methods 1), such that a tcGV containing only a few percent of FAsH-tagged GvpA would be sufficient for selective imaging.

GVs expressed in HEK 293T cells form clusters in the cytosol.

After demonstrating that intracellular tcGVs could be fluorescently labeled with FAsH, we sought to determine their subcellular location in mammalian cells. Knowledge of the localization of GVs within cells could improve our understanding of the biosynthesis and degradation of these protein structures and inform efforts to target GVs to specific organelles or cellular structures. Although phase contrast microscopy can be used to observe the presence of GVs within cells due to their differential refractive index,⁴⁴ it does not provide reliable information about their subcellular localization due to poor depth resolution. On the other hand, imaging the GVs using confocal microscopy, now enabled by FAsH labeling, would allow the determination of their precise subcellular location in 3D. To demonstrate this capability, we acquired multiple horizontal planes of cells expressing tcGVs labeled with FAsH and simultaneously stained the nucleus with DAPI and the plasma membrane with a membrane-trafficked fluorescent protein⁴⁵ (Lck-mScarlet-I) (Figure 2.4a; 3D renderings of additional cells are in Figure 2.S4).

After rendering the cells in 3D, we found that GVs form distinct clusters within the cell that vary considerably in size, ranging from the size of single GVs (around $0.003 \mu\text{m}^3$) to $20 \mu\text{m}^3$, with an average of $1.4 \mu\text{m}^3$ and a standard deviation of $2.9 \mu\text{m}^3$, and together occupy between 0.21% and 1.1% of the total cell volume. We then computed the distances between the GV clusters to the nuclear and plasma membranes and found that virtually all GV clusters were not in direct contact with the nucleus or the plasma membrane and remain localized to the cytosol, with the average GV cluster's center being $2.9 \pm 2.2 \mu\text{m}$ away from the nucleus and $2.6 \pm 0.92 \mu\text{m}$ away from the plasma membrane (Figure 2.4b-d).

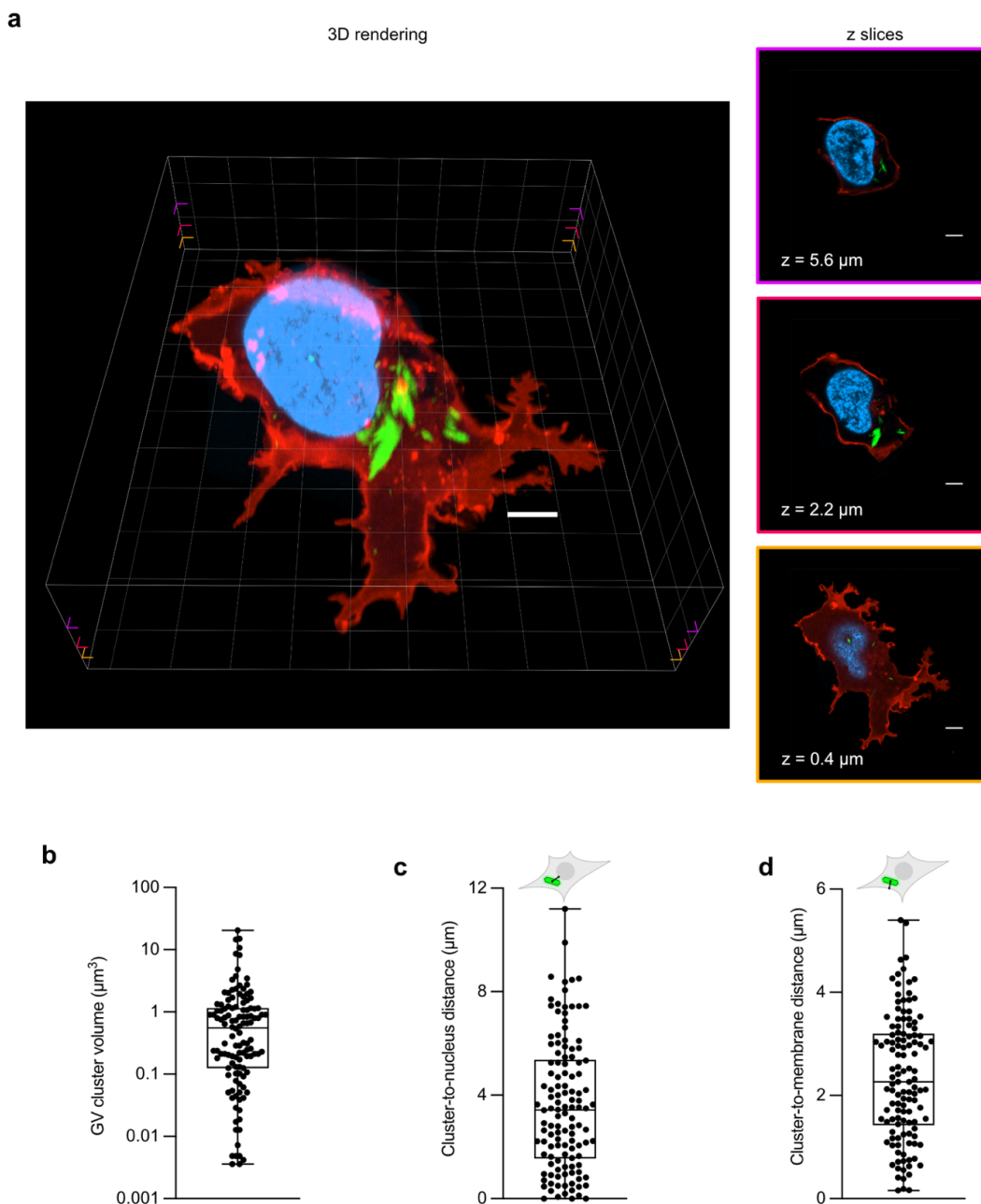


Figure 2.4: Fluorescence imaging of tcGVs elucidates the size and spatial distributions of GV clusters in HEK 293T cells. (a) A 3D rendering (left) of a fixed tcGV-expressing HEK 293T cell reacted with FIAsh. The membrane is shown in red (Lck-mScarlet-I), the nucleus in blue (DAPI), and tcGVs in green (FIAsh). All scale bars $5 \mu\text{m}$. Three z-slices of the 3D rendering are depicted at right. The border colors of the z-slices indicate the heights of the slices within the original 3D image: $z = 0.4 \mu\text{m}$ (orange, bottom), $z = 2.2 \mu\text{m}$ (red, middle), $z = 5.5 \mu\text{m}$ (purple, top) above the base of the cell. Corresponding notches in the 3D rendering mark the approximate heights of the z-slices. (b) – (d) Box-and-whiskers plots of the distributions of GV cluster volumes (b), distances to the nucleus (c), and distances to the membrane (d). $N = 6$ cells and 122 GV clusters analyzed.

2.4: Conclusion

In summary, our results show that intracellularly expressed GVs within HEK 293T cells can be fluorescently labeled and imaged with confocal microscopy for the first time. The C-terminus of GvpA proved to be quite tolerant of mutations to cysteine, allowing for the substitution of the TC tag into GvpA without major disruption of GV expression. And, while HEK 293T cells could not synthesize GVs made entirely of tcGvpA, we found that delivering a mixture of wtGvpA and tcGvpA led to the expression of FLAsH-labelable tcGVs. We demonstrated the utility of FLAsH labeling of in situ-expressed GVs by studying their intracellular distribution with higher spatial precision than ever before, and found that they generally localize to the cytoplasm. While in this study we used monocistronic co-transfection to deliver the tcGvpA and wtGvpA genes, we expect that this labeling approach could be improved with bicistronic expression where the two genes are linked using the IRES⁴⁶ sequence or the SEMPER system⁴⁷ to provide a finer control of their relative stoichiometry within the same cell. In addition, future studies of the relative protein composition of tcGvpA and wtGvpA within a tcGV as a function of gene ratio could inform the design of these multi-cistronic systems. We anticipate that our approach will become a tool that not only furthers the development of GV-based technologies, but also one that can be applied to the study of other genetically encoded polymeric proteinaceous structures.

2.5: Experimental methods

Expression and screening of Serratia GV variants in E. coli on solid media.

For the bacterial screens of the C-terminus of GvpA1, all mutants were cloned from the arabinose-inducible bARG_{ser} plasmid²⁷ (<https://www.addgene.org/192473/>) using Gibson assembly with enzyme mix (New England Biolabs, Ipswich, MA). A bacterial expression plasmid encoding GFP under the same promoter and backbone was used as a control in the same manner as the fluorescent protein controls described in Hurt et al.²⁷ The mutant plasmids were transformed via electroporation into Stable competent *E. coli* (New England Biolabs). Transformed *E. coli* were then plated onto solid inducer-free LB media containing

1.5% (w/v) agar, 1% (w/v) glucose, and 25 $\mu\text{g}/\text{mL}$ chloramphenicol. Bacterial patches were made by resuspending a colony of uninduced transformed *E. coli* in 100 μL phosphate-buffered saline (PBS), then depositing 1 μL of that suspension onto both an uninduced control plate and an induced LB media plate containing 1.5% (w/v) agar, 1% (w/v) L-arabinose, 0.1% (w/v) glucose, and 25 $\mu\text{g}/\text{mL}$ chloramphenicol using low-retention pipette tips. The bacterial patches were grown at 37 $^{\circ}\text{C}$ for 2 days. GV expression was quantified with a ChemiDoc gel imager (Bio-Rad, Hercules, CA) by measuring the opacity of the patches. Images were processed using ImageJ (NIH, Bethesda, MD). For each GvpA1 variant (and the GFP control), four separate transformed colonies were used to make patches in case of high patch-to-patch variability. Each of these four biological replicates was patch-plated four individual times: twice onto separate induced plates, and twice more onto separate uninduced plates.

Expression of GVs in HEK 293T cells.

HEK 293T cells (American Type Culture Collection [ATCC], CLR-2316) were cultured in a humidified incubator in 0.5 mL DMEM (Corning, 50-0030PC) with 10% FBS (Takara Bio, 631368) and 1x penicillin-streptomycin in 24-well glass-bottomed No. 0 plates (Mattek, Ashland, MA, P24G-0-10-F). The plates were pre-treated with 200 μL 50 $\mu\text{g}/\text{mL}$ fibronectin (Sigma-Aldrich, St. Louis, MO) in PBS at 37 $^{\circ}\text{C}$ overnight before the cells were added. When the cells reached around 40% confluency, they were transfected by mixing roughly 600 ng of plasmid mixture per well with 1.6 μL Transporter 5 Transfection Reagent (Polysciences, Warrington, PA) in 60 μL 150 mM NaCl, letting the DNA complexes form for 20 minutes, then gently pipetting the solution onto the cells. Cells were transfected with a modified mARG6 plasmid cocktail in which each GV gene was on its own plasmid driven by a constitutive cytomegalovirus (CMV) promoter. The plasmid cocktail contained a 4:1 molar ratio of wtGvpA to tcGvpA, no GvpC, a 4:1 molar ratio of total GvpA to every other individual GV gene, and an additional plasmid coding for Lck-mScarlet-I under a CMV promoter. For testing different ratios of wtGvpA to tcGvpA, the total GvpA concentration was kept constant and the relative molar ratio of the two plasmids was varied. Following

transfection, the growth media was exchanged daily until the cells grew fully confluent (usually on day 2 post-transfection); at this point, the cells were trypsinized and re-plated onto another fibronectin pre-treated 24-well plate at a 4x dilution of their original concentration. To achieve this, the growth media was aspirated and replaced with 50 μ L pre-warmed trypsin solution (Corning) per well, then the plate was incubated at 37 °C for 7 minutes. The trypsin was then quenched with 550 μ L DMEM per well; the contents of each well were then pipetted up and down, and 125 μ L of the new suspension was transferred into 375 μ L pre-warmed DMEM in a new plate for a 4x dilution. The new plate was then grown with daily media changes until the cells were roughly 60% confluent, at which point they were ready to be reacted with FIAsh.

FIAsh reaction of cultured HEK cells and preparation for imaging.

Live cultured cells were reacted with FIAsh by first washing with Hanks' Balanced Salt Solution (HBSS, Corning 21-023-CV), then applying 250 μ L of a 3 μ M working solution of FIAsh-EDT2 (Cayman Chemical, Ann Arbor, MI) in HBSS to each well. FIAsh-EDT2 aliquots were prepared at 2 mM in DMSO and frozen at -80 °C until use. The cells were stained with FIAsh for 30 minutes in the dark with the plate lid closed to prevent evaporation. After 30 minutes, the FIAsh working solution was removed and the cells were washed twice with a solution of 250 μ M dimercaprol (also known as British Anti-Lewisite, or BAL) to reduce non-specific FIAsh binding. Pure BAL (10 molar) was purchased from Sigma-Aldrich and diluted 400x in water to make a 25 mM stock solution. The stock solution was diluted 100x in HBSS to make the BAL working solution. After the second BAL wash, the cells were fixed with 2% paraformaldehyde (Electron Microscopy Sciences, Hatfield, PA) in PBS for 20 minutes, then stained with 1 μ g/mL DAPI.

Imaging and image processing of fixed, stained cells.

Cells were imaged with a Zeiss LSM 800 confocal microscope with ZEN Blue. Images were processed with the Fiji package of ImageJ. 3D renderings and measurements were performed with Imaris 10.0.1 software (Oxford Instruments, Abingdon, England, United Kingdom). In

Imaris, strongly fluorescent regions in 3D space were treated as surfaces; regions of green fluorescence corresponded to tcGVs (FIAsH), red to the membrane (mScarlet-I), and blue to the nucleus (DAPI). The software was used to compute statistics relevant to these surfaces, such as the distances between them, their total volume, etc. Distances between the GV clusters and the nucleus and membrane were calculated from the distance between the estimated geometric center of each GV cluster and the nearest point on the relevant surface (nucleus/membrane).

2.6: Acknowledgements

Imaging was performed in the Biological Imaging Facility, with the support of the Caltech Beckman Institute and the Arnold and Mabel Beckman Foundation. The authors particularly thank Dr. Giada Spigolon of the Biological Imaging Facility for her assistance with the confocal microscopy and 3D rendering of the z-stacks. This work was supported by the Chan-Zuckerberg Initiative (2020-225370 to MGS) and the National Institutes of Health (DP1 EB033154 to MGS). Related work in the Shapiro lab is supported by the David and Lucile Packard Foundation. MGS is an investigator of the Howard Hughes Medical Institute.

2.7: References

- (24) Dutka, P.; Metskas, L. A.; Hurt, R. C.; Salahshoor, H.; Wang, T.-Y.; Malounda, D.; Lu, G. J.; Chou, T.-F.; Shapiro, M. G.; Jensen, G. J. Structure of *Anabaena Flos-Aquae* Gas Vesicles Revealed by Cryo-ET. *Structure* **2023**, *31* (5), 518-528.e6. <https://doi.org/10.1016/j.str.2023.03.011>.
- (26) Bourdeau, R. W.; Lee-Gosselin, A.; Lakshmanan, A.; Farhadi, A.; Kumar, S. R.; Nety, S. P.; Shapiro, M. G. Acoustic Reporter Genes for Noninvasive Imaging of Microorganisms in Mammalian Hosts. *Nature* **2018**, *553* (7686), 86–90. <https://doi.org/10.1038/nature25021>.
- (27) Hurt, R. C.; Buss, M. T.; Duan, M.; Wong, K.; You, M. Y.; Sawyer, D. P.; Swift, M. B.; Dutka, P.; Barturen-Larrea, P.; Mittelstein, D. R.; Jin, Z.; Abedi, M. H.; Farhadi, A.; Deshpande, R.; Shapiro, M. G. Genomically Mined Acoustic Reporter Genes for

- Real-Time in Vivo Monitoring of Tumors and Tumor-Homing Bacteria. *Nat. Biotechnol.* **2023**, *41* (7), 919–931. <https://doi.org/10.1038/s41587-022-01581-y>.
- (28) Lakshmanan, A.; Jin, Z.; Nety, S. P.; Sawyer, D. P.; Lee-Gosselin, A.; Malounda, D.; Swift, M. B.; Maresca, D.; Shapiro, M. G. Acoustic Biosensors for Ultrasound Imaging of Enzyme Activity. *Nat. Chem. Biol.* **2020**, *16* (9), 988–996. <https://doi.org/10.1038/s41589-020-0591-0>.
- (29) Bar-Zion, A.; Nourmahnad, A.; Mittelstein, D. R.; Shivaiei, S.; Yoo, S.; Buss, M. T.; Hurt, R. C.; Malounda, D.; Abedi, M. H.; Lee-Gosselin, A.; Swift, M. B.; Maresca, D.; Shapiro, M. G. Acoustically Triggered Mechanotherapy Using Genetically Encoded Gas Vesicles. *Nat. Nanotechnol.* **2021**, *16* (12), 1403–1412. <https://doi.org/10.1038/s41565-021-00971-8>.
- (30) Wu, D.; Baresch, D.; Cook, C.; Ma, Z.; Duan, M.; Malounda, D.; Maresca, D.; Abundo, M. P.; Lee, J.; Shivaiei, S.; Mittelstein, D. R.; Qiu, T.; Fischer, P.; Shapiro, M. G. Biomolecular Actuators for Genetically Selective Acoustic Manipulation of Cells. *Sci. Adv.* **2023**, *9* (8), eadd9186. <https://doi.org/10.1126/sciadv.add9186>.
- (32) Sigmund, F.; Berezin, O.; Beliakova, S.; Magerl, B.; Drawitsch, M.; Piovesan, A.; Gonçalves, F.; Bodea, S.-V.; Winkler, S.; Bousraou, Z.; Grosshauser, M.; Samara, E.; Pujol-Martí, J.; Schädler, S.; So, C.; Irsen, S.; Walch, A.; Kofler, F.; Piraud, M.; Kornfeld, J.; Briggman, K.; Westmeyer, G. G. Genetically Encoded Barcodes for Correlative Volume Electron Microscopy. *Nat. Biotechnol.* **2023**. <https://doi.org/10.1038/s41587-023-01713-y>.
- (33) Mohsen, M. O.; Bachmann, M. F. Virus-like Particle Vaccinology, from Bench to Bedside. *Cell. Mol. Immunol.* **2022**, *19* (9), 993–1011. <https://doi.org/10.1038/s41423-022-00897-8>.
- (34) Edwardson, T. G. W.; Mori, T.; Hilvert, D. Rational Engineering of a Designed Protein Cage for siRNA Delivery. *J. Am. Chem. Soc.* **2018**, *140* (33), 10439–10442. <https://doi.org/10.1021/jacs.8b06442>.
- (35) Ling, B.; Lee, J.; Maresca, D.; Lee-Gosselin, A.; Malounda, D.; Swift, M. B.; Shapiro, M. G. Biomolecular Ultrasound Imaging of Phagolysosomal Function. *ACS Nano* **2020**, *14* (9), 12210–12221. <https://doi.org/10.1021/acsnano.0c05912>.

- (36) Jin, Z.; Lakshmanan, A.; Zhang, R.; Tran, T. A.; Rabut, C.; Dutka, P.; Duan, M.; Hurt, R. C.; Malounda, D.; Yao, Y.; Shapiro, M. G. *Ultrasonic Reporters of Calcium for Deep Tissue Imaging of Cellular Signals*; preprint; 2023. <https://doi.org/10.1101/2023.11.09.566364>.
- (37) Griffin, B. A.; Adams, S. R.; Tsien, R. Y. Specific Covalent Labeling of Recombinant Protein Molecules Inside Live Cells. *Science* **1998**, *281* (5374), 269–272. <https://doi.org/10.1126/science.281.5374.269>.
- (38) Adams, S. R.; Campbell, R. E.; Gross, L. A.; Martin, B. R.; Walkup, G. K.; Yao, Y.; Llopis, J.; Tsien, R. Y. New Biarsenical Ligands and Tetracysteine Motifs for Protein Labeling in Vitro and in Vivo: Synthesis and Biological Applications. *J. Am. Chem. Soc.* **2002**, *124* (21), 6063–6076. <https://doi.org/10.1021/ja017687n>.
- (39) Martin, B. R.; Giepmans, B. N. G.; Adams, S. R.; Tsien, R. Y. Mammalian Cell–Based Optimization of the Biarsenical-Binding Tetracysteine Motif for Improved Fluorescence and Affinity. *Nat. Biotechnol.* **2005**, *23* (10), 1308–1314. <https://doi.org/10.1038/nbt1136>.
- (40) Hoffmann, C.; Gaietta, G.; Zürn, A.; Adams, S. R.; Terrillon, S.; Ellisman, M. H.; Tsien, R. Y.; Lohse, M. J. Fluorescent Labeling of Tetracysteine-Tagged Proteins in Intact Cells. *Nat. Protoc.* **2010**, *5* (10), 1666–1677. <https://doi.org/10.1038/nprot.2010.129>.
- (41) Huber, S. T.; Terwiel, D.; Evers, W. H.; Maresca, D.; Jakobi, A. J. Cryo-EM Structure of Gas Vesicles for Buoyancy-Controlled Motility. *Cell* **2023**, *186* (5), 975–986.e13. <https://doi.org/10.1016/j.cell.2023.01.041>.
- (42) Lakshmanan, A.; Farhadi, A.; Nety, S. P.; Lee-Gosselin, A.; Bourdeau, R. W.; Maresca, D.; Shapiro, M. G. Molecular Engineering of Acoustic Protein Nanostructures. *ACS Nano* **2016**, *10* (8), 7314–7322. <https://doi.org/10.1021/acsnano.6b03364>.
- (43) Lu, G. J.; Chou, L.; Malounda, D.; Patel, A. K.; Welsbie, D. S.; Chao, D. L.; Ramalingam, T.; Shapiro, M. G. Genetically Encodable Contrast Agents for Optical Coherence Tomography. *ACS Nano* **2020**, *14* (7), 7823–7831. <https://doi.org/10.1021/acsnano.9b08432>.

- (44) Farhadi, A.; Bedrossian, M.; Lee, J.; Ho, G. H.; Shapiro, M. G.; Nadeau, J. L. Genetically Encoded Phase Contrast Agents for Digital Holographic Microscopy. *Nano Lett.* **2020**, *20* (11), 8127–8134. <https://doi.org/10.1021/acs.nanolett.0c03159>.
- (45) Zlatkine, P.; Mehul, B.; Magee, A. I. Retargeting of Cytosolic Proteins to the Plasma Membrane by the Lck Protein Tyrosine Kinase Dual Acylation Motif. *J. Cell Sci.* **1997**, *110* (5), 673–679. <https://doi.org/10.1242/jcs.110.5.673>.
- (46) Pelletier, J.; Sonenberg, N. Internal Initiation of Translation of Eukaryotic mRNA Directed by a Sequence Derived from Poliovirus RNA. *Nature* **1988**, *334* (6180), 320–325. <https://doi.org/10.1038/334320a0>.
- (47) Duan, M.; Dev, I.; Lu, A.; Ayrapetyan, G.; You, M. Y.; Shapiro, M. G. SEMPER: Stoichiometric Expression of mRNA Polycistrons by Eukaryotic Ribosomes for Compact, Ratio-Tunable Multi-Gene Expression. *Cell Syst.* **2024**, *15* (7), 597-609.e4. <https://doi.org/10.1016/j.cels.2024.06.001>.

2.8: Supporting information

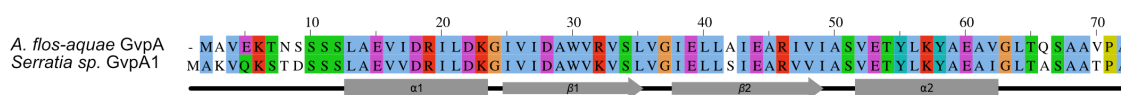


Figure 2.S1: Sequence alignment for *Anabaena flos-aquae* gvpA and *Serratia* sp. 39006 gvpA1. The two genes have an identity score of 80.6% (58 of 72 amino acids) and a similarity score of 91.7% (66 of 72 amino acids). Colored amino acids represent pairs of amino acids with similar or identical side chains: blue for hydrophobic groups, purple for negatively charged groups, green for polar uncharged groups, red for positively charged groups, orange for glycine, teal for aromatic groups (tyrosine and histidine), and yellow for proline.

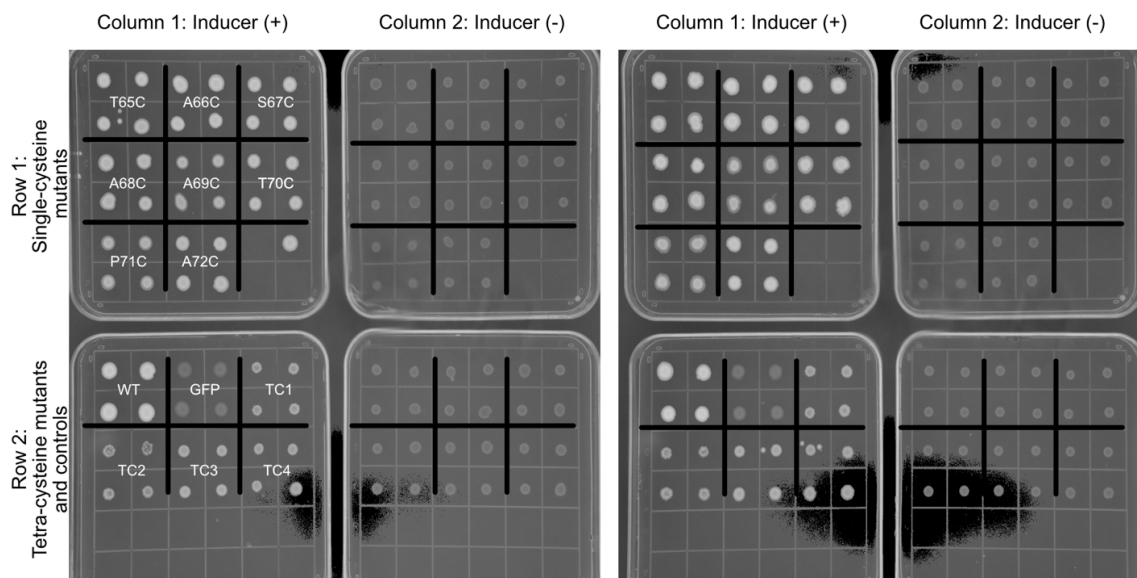


Figure 2.S2: Opacity screen of mutant *gvpA1* plasmids in *E. coli*. Patches of *E. coli* transformed with arabinose-inducible constructs encoding mutant *gvpA1*, wild type *gvpA1*, or GFP were grown on LB agar plates. Two images, each showing a set of four distinct plates, are shown. The patches on the four plates on the right represent duplicate technical replicates of the corresponding patches on the four plates on the left. Within each set of four plates, the two plates on the left (column 1) contain the inducer arabinose; the two plates on the right (column 2) do not. Each *gvpA1* variant (and GFP) is represented by 4 patches arranged into a 2x2 grid in which each of the 4 patches originates from a different colony from the original transformation (i.e., each of the 4 patches represents a distinct biological replicate). 2x2 grids of patches are labeled with their corresponding *gvpA1* variant (or GFP) in the column on the left; all other columns are arranged identically.

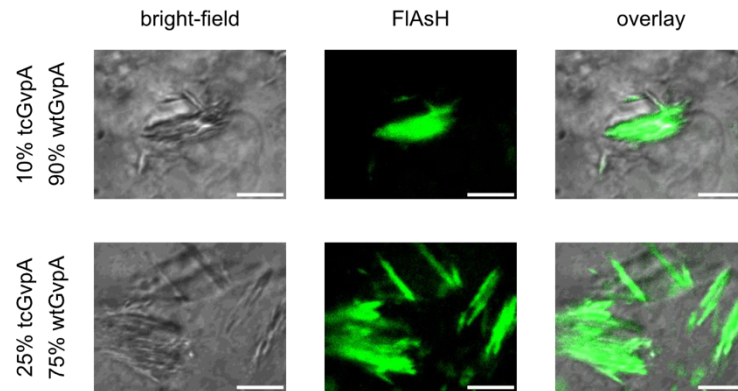


Figure 2.S3: Images of FIAsh-labeled GVs in cells transfected with different ratios of wtGvpA:tcGvpA. Images of tcGV clusters in fixed HEK 293T cells transfected with 10% (top row) and 25% (bottom row) tcGvpA. GV clusters are visible under bright-field imaging (first column) and are brightly labeled with FIAsh (second column). The bright-field/FIAsh overlay (third column) demonstrates that the strongest FIAsh signal overlaps with tcGV clusters. All scale bars 5 μm . Cells transfected with 100% tcGvpA did not result in visible GV formation (data not shown).

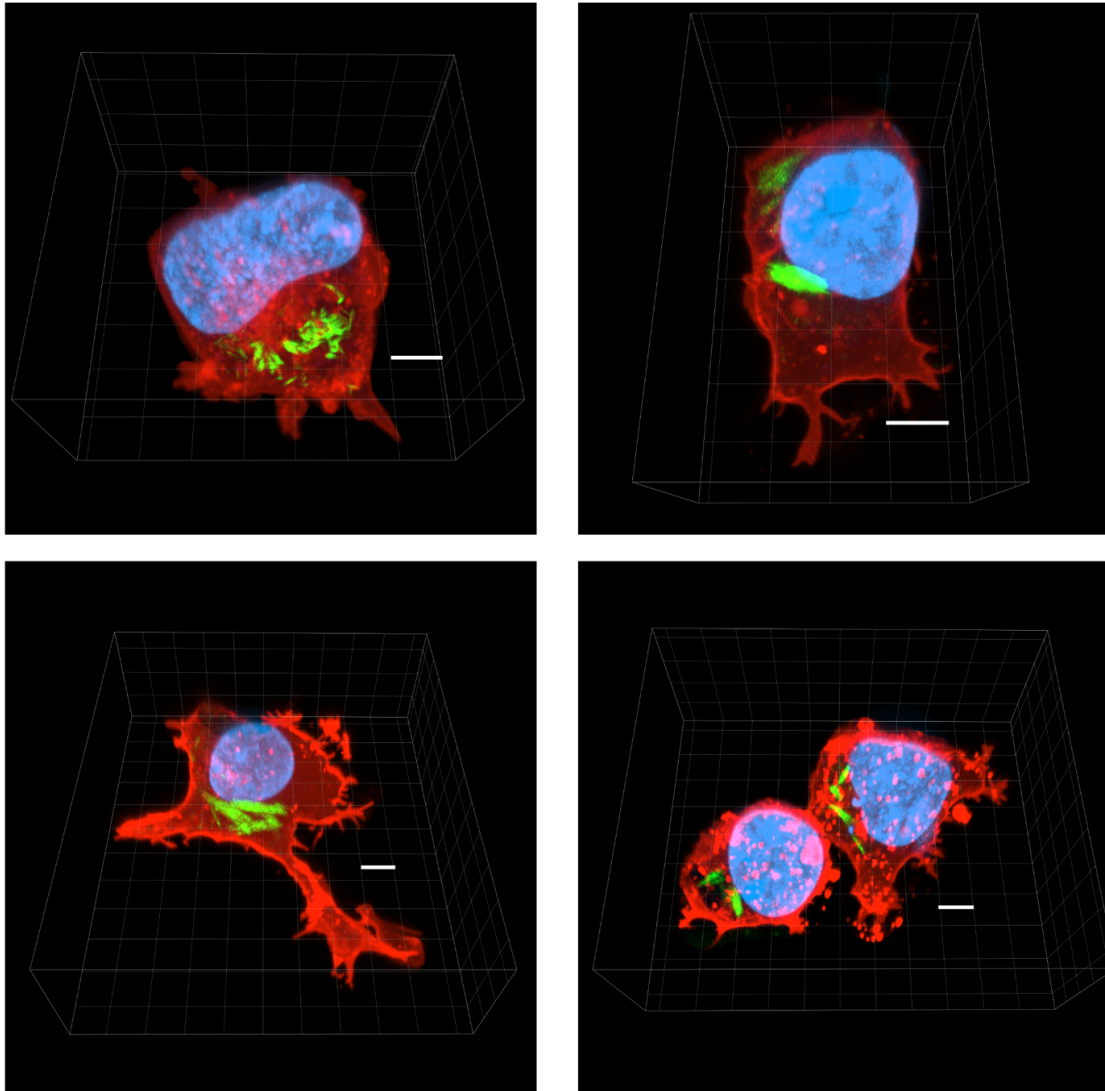


Figure 2.S4: 3D renderings of tcGV-expressing cells. The cell membrane is depicted in red (Lck-mScarlet-I), tcGVs in green (FlAsH), and nucleus in blue (DAPI). All scale bars 5 μm .

Supplementary Methods 1: Estimation of the GvpA concentration within a typical FLAsH imaging voxel.

To estimate the molar concentration of GvpA in a typical imaging voxel, we first estimated the number of GvpA molecules in a typical GV (n_{GvpA}) using the length of a typical *Anabaena flos-aquae* GV ($L = 500$ nm), the number of GvpA per helical turn ($n = 227$) (ref. 24), and the helical pitch ($P = 4.9$ nm) (ref. 41) as follows:

$$n_{GvpA} = n * \frac{L}{P} \approx 2 \times 10^4.$$

Assuming a typical imaging voxel of $(500 \text{ nm})^3$ for FLAsH imaging, a single GV within the voxel would result in a GvpA concentration of $\sim 300 \mu\text{M}$. A tightly packed GV cluster within the voxel would give a GvpA concentration of $\sim 10 \text{ mM}$.

References (see Section 2.7):

- (24) Dutka, P.; Metskas, L. A.; Hurt, R. C.; Salahshoor, H.; Wang, T.-Y.; Malounda, D.; Lu, G. J.; Chou, T.-F.; Shapiro, M. G.; Jensen, G. J. Structure of *Anabaena Flos-Aquae* Gas Vesicles Revealed by Cryo-ET. *Structure* **2023**, *31* (5), 518-528.e6. <https://doi.org/10.1016/j.str.2023.03.011>.
- (41) Huber, S. T.; Terwiel, D.; Evers, W. H.; Maresca, D.; Jakobi, A. J. Cryo-EM Structure of Gas Vesicles for Buoyancy-Controlled Motility. *Cell* **2023**, *186* (5), 975-986.e13. <https://doi.org/10.1016/j.cell.2023.01.041>.

SONO-UNCAGING OF ENGINEERED GAS VESICLES FOR SPATIOTEMPORAL CONTROL OF THIOL REACTIVITY

Schrunk, E.; Lee, S.; Dutka, P.; Wu, D.; Shapiro, M. G. Sono-Uncaging of Engineered Gas Vesicles for Spatiotemporal Control of Thiol Reactivity. *Manuscript in preparation.*

3.1: Abstract

Photo-uncaging—the use of light to reveal the active part of a chemical compound by photolysis of a protecting group—has long been used to study and actuate biochemical processes. However, light scattering limits the applications of photo-uncaging in opaque specimens or tissues. Here, we introduce sono-uncaging, a process in which a chemical functional group becomes exposed upon administration of ultrasound (US), which can be applied and focused in optically opaque materials. We engineered gas vesicles (GVs), air-filled protein nanostructures sensitive to US, to contain cysteines on their concealed inner surface, hypothesizing that the application of US would collapse the GV shell and reveal the cysteines. The resulting SonoCage construct reacted with monobromobimane (mBBr), a fluorogenic, thiol-reactive molecule, only after treatment with US, establishing the sono-uncaging proof of concept. We then demonstrated the spatial patterning capability of sono-uncaging by embedding the SonoCages in an mBBr-containing hydrogel and creating fluorescent patterns with holographic US. This patterning could be accomplished using a diagnostic imaging transducer. This work establishes sono-uncaging as a method for spatiotemporal control over chemical reactivity using widely available ultrasound technology.

3.2: Introduction

In biology, photochemical uncaging is commonly used to control the activity of ions,^{5,48,49} neurotransmitters,^{50–52} proteins and peptides,^{53–55} nucleic acids,^{6,56,57} and other bio-interactive compounds.^{7,55,58} However, due to light scattering and absorption, photocaged systems have limited utility in opaque biological specimens or tissues.

Unlike light, ultrasound (US) provides centimeter-scale penetration depth into opaque materials, where it can be focused with sub-millimeter spatial precision. US has been used to control chemical reactions via cavitation-driven mechanical forces on mechanophores^{59–61} or the generation of reactive oxygen species.^{62–64} However, the conditions commonly used to elicit cavitation effects can be harmful to tissues and require specialized focused ultrasound equipment,^{59,65} limiting the utility of existing US-triggered chemistries in living systems.

In this study, we set out to establish control of biochemical functions using mild, non-cavitating US that can be applied using common imaging devices (Figure 3.1a). Our approach takes advantage of gas vesicles (GVs), genetically encodable air-filled protein nanostructures (~85 nm diameter, ~500 nm length)²⁴ that have recently emerged as the first biomolecular agents for US imaging and actuation. (Figure 3.1b). The stark density and compressibility differences between GV's air-filled interiors and their aqueous surroundings endow these nanoparticles with strong US contrast. Meanwhile, their biocompatibility, engineerability and genetic encodability have enabled their use in a variety of biological scenarios.^{27,36,66,67} One aspect of GV's interaction with US is that they mechanically collapse under acoustic pressure above a certain pressure threshold. This collapse results in the partial exposure of their shell interior, which is normally shielded from aqueous media.

Here, we describe SonoCages, which reveal a reduced thiol moiety only after application of mild US—a process we call “sono-uncaging.” SonoCages are GV's with an inward-facing cysteine substitution to their shell protein GvpA1: the cysteine's thiol side chain is

hidden in the air-filled GV interior and can only be accessed once the GVs are collapsed by US and their interiors exposed to the surrounding environment. We identified this key mutation using a combination of structural predictions and a cysteine scanning mutant library. The library scan generated a catalog of cysteine-tolerant amino acid sites, which we compared against the list of sites whose side chains were predicted to face inward; this resulted in four potentially inward-facing cysteine mutants. We moved forward with the best-expressing of the mutants, V47C, and demonstrated that those GVs could undergo US-activated exposure of cysteine (sono-uncaging) by reacting them with monobromobimane (mBBR), a molecule that reacts with reduced thiols and which becomes fluorescent upon reaction,⁶⁸ thereby validating the sono-uncaging proof of concept and establishing V47C mutant GVs as SonoCages. Next, we used mild, biocompatible US to generate sub-centimeter-scale patterns in agarose hydrogels containing SonoCages and mBBR. We observed that mBBR fluorescence was confined to regions of collapsed SonoCages. Thus, these SonoCages represent a spatially, temporally controllable source of a chemically reactive group that can be activated through US.

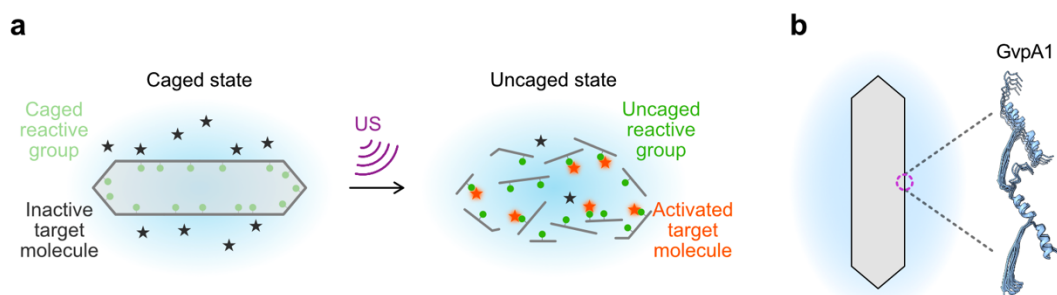


Figure 3.1: Sono-uncaging and SonoCages. (a) Schematic of sono-uncaging. The caged state encloses the reactive group (green dot) within the air-filled interior of the SonoCage. A target molecule (star) that reacts with the caged group is in solution, physically separated from the caged groups by the GV walls. After application of ultrasound (US), the reactive group is uncaged and free to react with the target molecule. (Reacted or “activated” target molecule depicted in orange.) (b) SonoCages are engineered from GVs (left), which are composed of repeating units of the structural protein GvpA1 (right).

3.3 Results and discussion

Several internal-facing residues in GvpA1 are tolerant to mutations to cysteine.

To develop sono-uncageable GVs, we sought to introduce a unique chemical group into GVs' interior walls such that the chemical moiety would only be exposed (uncaged) once the GVs are collapsed. We chose to uncage cysteine for several reasons. First, as a natural amino acid, cysteine can be readily incorporated into the GV shell by endogenous translation machinery. Second, of the natural amino acids, cysteine is the only molecule to possess the thiol functional group, which participates in rather unique chemical reactions (thiol-maleimide, thiol-iodoacetamide, etc.) compared to other amino acids, allowing for cysteine-specific applications and assays. Finally, wild-type (WT) GvpA1 does not contain cysteine, meaning that WT GVs are not able to undergo sono-uncaging of cysteine and can serve as cysteine-free controls.

To introduce cysteine into the GVs' interior walls, we cross-referenced predicted interior-facing residues of GvpA1 with experimentally determined cysteine-tolerant amino acid sites to arrive at a short list of potential sono-uncaging candidates. In brief, we set up a cysteine scanning mutant plasmid library of gvpA1 and transformed those plasmids in bulk into *E. coli*, which we then plated onto inducer-containing agar dishes. We used the opacity of induced colonies as a proxy for GV expression (as GV-expressing colonies look white) to identify the cysteine mutations that do not abrogate GV expression; we next compared those cysteine-tolerant sites with the positions of side chains predicted to be inward-facing (Figure 3.2a) from the structure of the highly related protein GvpA²⁴ (~92% similarity to GvpA1, sequence alignment in Figure 3.S1). That search yielded four mutants—V16C, V17C, V33C, and V47C—that both expressed GVs and were expected to have interior-facing thiol groups (Figure 3.2b-d). To compare their relative expression levels, we expressed all four mutant GV variants alongside WT GVs and green fluorescent protein (GFP) in replicate bacterial patches (Figure 3.2e, 3.S2). We moved forward with the best-expressing variant, V47C, as our top candidate for SonoCages.

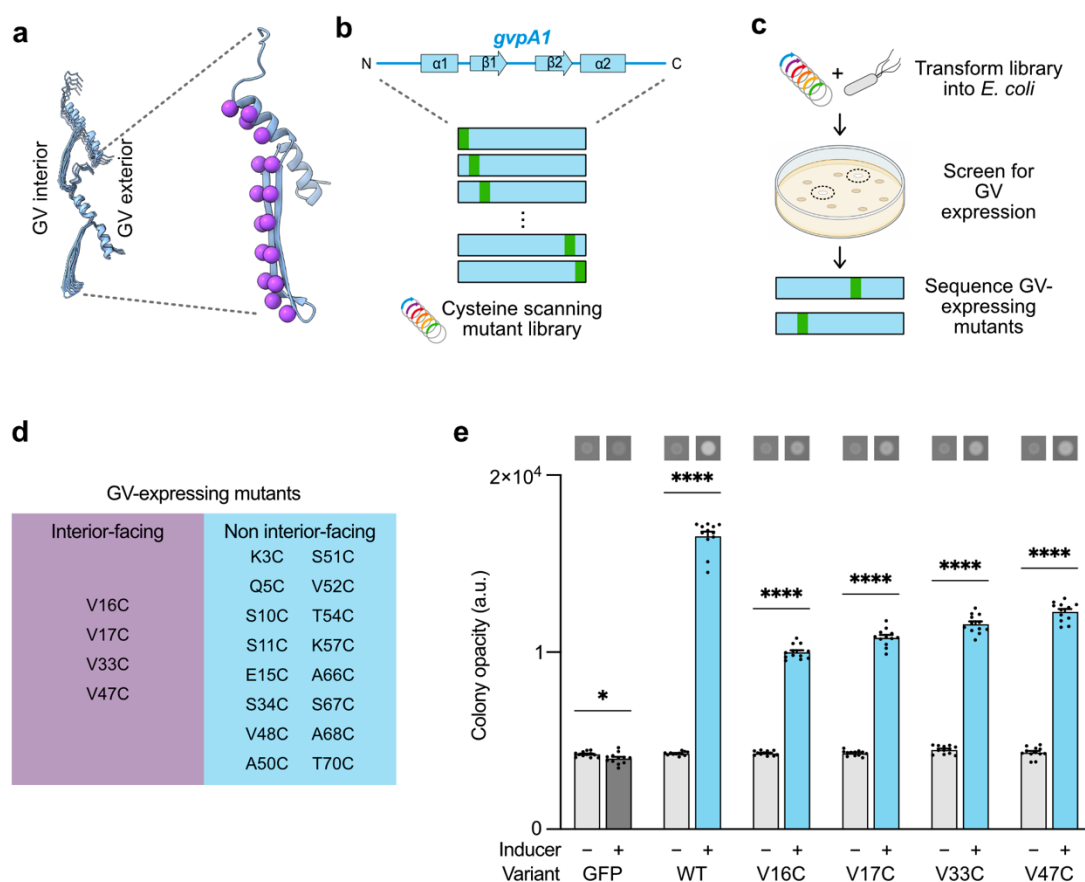


Figure 3.2: GvpA1 cysteine scanning library identifies several SonoCage candidates with potentially inward-facing cysteine side chains. (a) Schematic of GV shell (left) with GV interior and exterior regions shown. Single GvpA1 protein (right) with predicted interior-facing side chains highlighted in purple. (b) A cysteine scanning mutant library for the *gvpA1* gene that codes for GvpA1, the primary structural protein in GVs. (c) Workflow for the development of a cysteine-enclosing SonoCage. The cysteine scanning mutant library was transformed into *E. coli* and GV expression was induced. Colonies that turned white were treated as GV-expressing and sequenced. (d) Diagram depicting the predicted side chain orientation of all GV-expressing cysteine mutants discovered. Candidates for sono-uncaging of cysteine are on the left (in purple). (e) Graph of opacity for uninduced and induced bacterial patches transformed with plasmids encoding mutant GV expression. Colony opacity is indicative of GV expression. Representative images of uninduced and induced patches are displayed above their corresponding columns in the graph. N = 12 patches per condition. Patches with a plasmid encoding green fluorescent protein (GFP) expression were included as a GV-negative control. Asterisks represent statistical significance by unpaired t-tests (****: $p < 0.0001$, *: $p < 0.05$). Error bars represent mean \pm SEM. The V33C mutant is a double mutant, with an additional mutation at A50.

V47C mutant GVs demonstrate sono-uncaging in response to collapse triggered by US.

Next, we tested our hypothesis that V47C serratia GVs could undergo sono-uncaging of cysteine. We incubated the GVs with monobromobimane (mBBr), a molecule that reacts with reduced thiol under biological conditions and drastically increases fluorescence, and observed that the V47C GVs experienced a very large relative increase in mBBr fluorescence after administration of US compared to the WT GV controls in both PBS (Figure 3.3b) and 0.5% low-melt agarose (Figure 3.3c). We then imaged WT- and V47C-containing samples in PBS with confocal microscopy and similarly found that only the US-treated V47C sample exhibited higher-than-background mBBr fluorescence (Figure 3.S3). These results confirmed that V47C mutant GVs could undergo sono-uncaging in solution—we had indeed developed SonoCages.

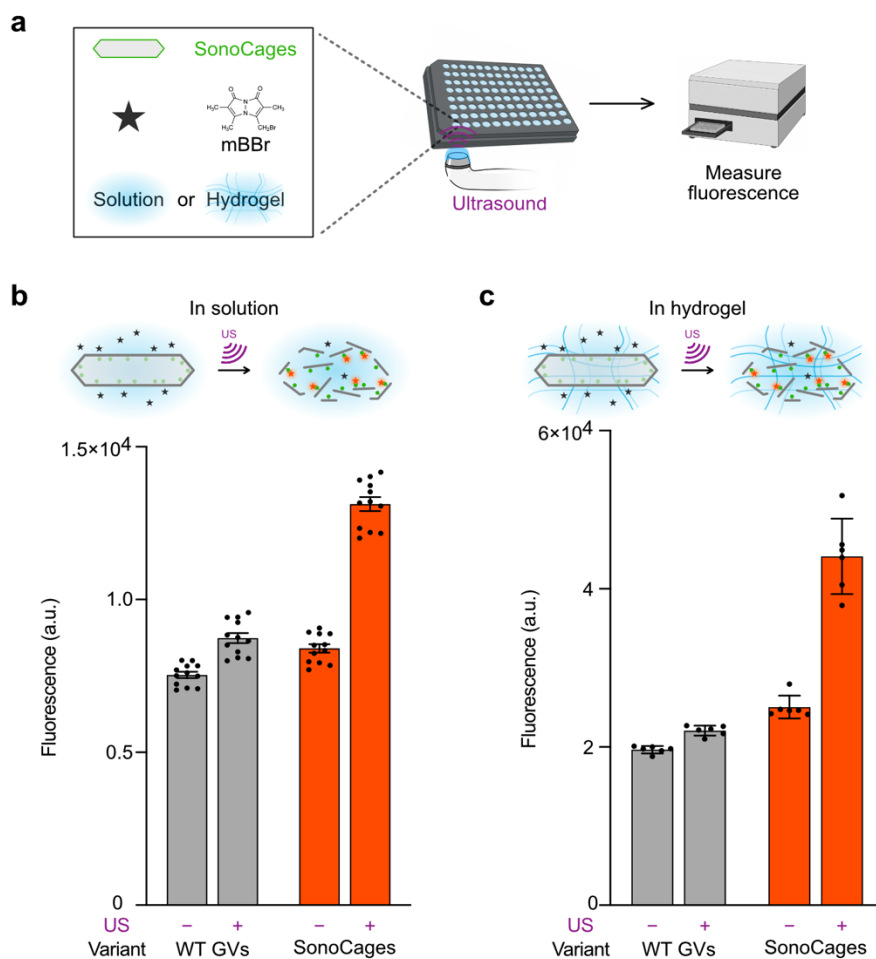


Figure 3.3: SonoCages (V47C mutant GVs) undergo sono-uncaging of cysteine in solution and in agarose hydrogels. (a) Schematic of process flow for sono-uncaging proof-of-concept experiments. (b) Graph of mBBr fluorescence for WT GV and SonoCage samples in PBS. In each pair of columns, the right column received US whereas the left did not. N = 12 wells of a 96-well plate per condition. (c) Graph of mBBr fluorescence for WT GV and SonoCage samples in a 0.5% w/v low-melt agarose hydrogel. In each pair of columns, the right column received US whereas the left did not. N = 6 wells of a 96-well plate per condition.

SonoCages allow for spatiotemporal control of thiol reactivity.

After validating the sono-uncaging proof of concept with our SonoCages, we demonstrated their utility by using US to create a desired spatial pattern of reactivity in 2 dimensions. We prepared a 0.25% agarose hydrogel containing SonoCages and used US to collapse the GVs in a pattern (Figure 3.4a). Specifically, we generated a focused beam (transmit frequency = 8.9 MHz, focal length = 7 mm, number of half-cycles = 10, steering angle = 0°) using 8 x 8 elements from a matrix array probe (32 x 32 elements, center frequency = 15 MHz, pitch size = 0.3 mm) at each desired location based on patterns drawn on a 25 x 25 binary grid. The input voltages to the transducer were 25 V and 20 V for WT GV and SonoCage samples, respectively. Under confocal microscopy, the mBBr fluorescent pattern corresponded to regions of collapse; a similarly patterned WT GV control did not exhibit the same degree of fluorescence (Figure 3.4b). We tried several other patterns, all of which behaved similarly (Figure 3.4c). These results underscore the advantage of sono-uncaging: mild US effected a chemical reaction in a predetermined pattern with sub-centimeter precision. While in this experiment fluorescence was used as the readout for the thiol-mBBr reaction, this same approach could be used to pattern thiol reactivity in opaque media. Furthermore, the relative ease of using US to create the pattern also suggests that this method can be used even in cases where biocompatibility and high penetration depth are not both needed, such as in matrigels or in large volumes of hydrogel that do not contain cells.

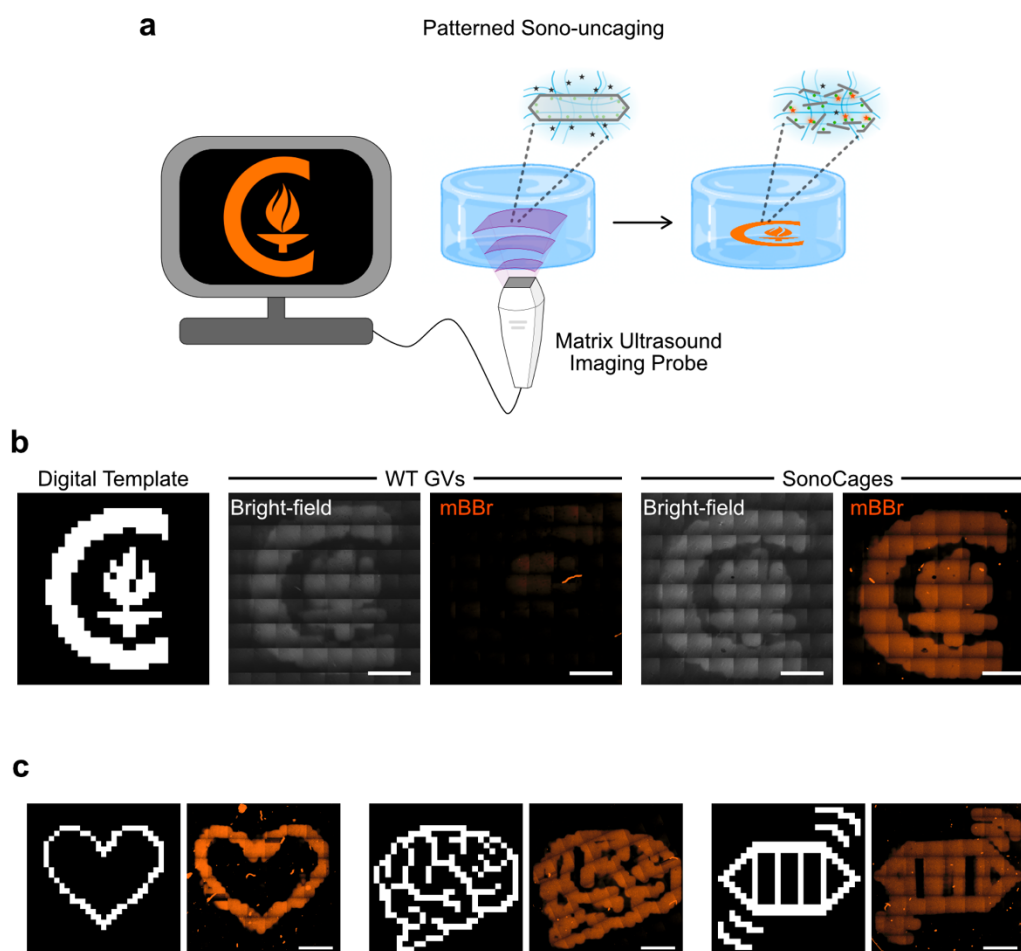


Figure 3.4: Sono-uncaging of SonoCages leads to patterning of thiol reactivity with spatiotemporal control in an agarose gel. (a) Schematic for US patterning of thiol reactivity. An agarose hydrogel containing intact SonoCages and mBBR was prepared. US was used to create a Caltech logo pattern of collapsed GVs, leading to thiol exposure and reaction with mBBR only in areas of GV collapse. (b) Confocal images of Caltech logo patterns in 0.25% low-melt agarose with 10 μ M mBBR and either WT GVs or SonoCages. All scale bars 2 mm. (c) Confocal mBBR fluorescence images of SonoCage samples with other patterns. All scale bars 2 mm.

3.4 Conclusion

Taken together, these results illustrate the novel use of mild, bio-compatible US to exert spatiotemporal control over chemical reactivity with SonoCages. Our cysteine mutant library screen revealed that, while quite a few amino acids in GvpA1 could individually be mutated to cysteine without abrogating GV expression, only a few of those sites were also

likely inward facing. Of those mutants, the V47C variant expressed the best; we purified those GVs and found that these SonoCages reacted with a fluorogenic, thiol-reactive compound after application of US. Furthermore, we used mild US to create sub-centimeter-scale patterns in a SonoCage-containing agarose gel and found that fluorescence, and thus thiol reactivity, was localized to areas of GV collapse.

While in this study we demonstrated the sono-uncaging of reduced thiol, we believe that our approach can be generalized to any reactive amino acid side chain. Given the vast range of chemical groups in non-canonical amino acids,^{69,70} sono-uncaging could be used to trigger a wide variety of reactions for many diverse applications; a simple mutant expression screen in an appropriate bacterial strain could yield the desired SonoCage. Additionally, as they are based on GVs, SonoCages bearing any chemical group could be used for many of the original applications of GVs prior to their collapse. With the recent development of multiplexed GV imaging⁶⁶ based on the engineering of GVs with different acoustic properties, sono-uncaging could even be used to serially activate disparate chemistries in mixed populations of SonoCages with different reactive moieties. We believe that our findings establish SonoCages and sono-uncaging as a platform for controlling reactivity with ultrasound, and we hope that this approach can be extended to different chemical groups, customized to the user's needs, and used wherever US is necessary or convenient.

3.5 Experimental methods

Design, assembly, and screening of GvpA1 cysteine scanning mutant library.

The cysteine scanning GvpA1 library was constructed in a manner similar to the scanning site saturation libraries described by Hurt et al.⁷¹ except that each amino acid in GvpA1 was mutated to only cysteine. The arabinose-inducible bARG_{Ser} plasmid,²⁷ which contains the *gvpA1* gene under the control of the pBAD promoter, was used as the starting point for the mutant library construction. *gvpA1* was divided into three subunits that tiled the gene, and three oligo libraries were designed such that each library contained a middle variable

region covering one subunit of the gene plus two invariable anchoring regions on either side of the variable region. The variable region substituted each codon individually to TGT (cysteine); the anchoring regions were used as primer binding sites in the PCR amplification of the oligo libraries and as overlapping regions in the Gibson assembly of the mutant plasmids as described below. These oligo libraries were synthesized as one oligo pool by Twist Bioscience. The three oligo libraries were then amplified from the pool with PCR using primers designed for each library's anchoring regions. Only 14 total cycles of PCR were used to lower the risks of mutation swapping and of any one oligo dominating the library. The amplified oligo libraries were isolated by electrophoresis using a 3% agarose gel with TBE (tris-borate-EDTA) buffer and purified with a New England Biolabs ("NEB"; Ipswich, MA) DNA cleanup column. The three oligo pools were assembled into mutant plasmid libraries via Gibson assembly (NEB); the anchoring regions of the oligos served as the overlaps between the oligos and the corresponding backbone fragments as well as the binding sites of the PCR primers used to amplify those backbone fragments. The three mutant plasmid libraries were then transformed into NEB Stable electrically competent cells and plated onto solid agar media in either inducing (1% L-arabinose and 0.1% glucose) or non-inducing (1% glucose, no arabinose) conditions. Colonies that appeared white (indicating GV expression) on the induced plate were minipreped and sequenced.

GV interior-cysteine candidate expression screen.

GV-expressing cysteine variants identified in the cysteine scanning library were then cross-referenced with GvpA1 amino acid sites believed to be interior-facing (Figure 3.2d), leading to four potential interior-cysteine candidates. The candidate variants' relative GV expression levels were compared using an opacity-based assay of GV-expressing bacterial patches very similar to our previous work (cite FLASH paper). The four mutant plasmids, along with a plasmid encoding WT GvpA1 and a plasmid encoding GFP under the same promoter, were transformed into NEB Stable electrically competent cells via electroporation. Transformed *E. coli* were then plated onto solid inducer-free LB media

containing 1.5% (w/v) agar, 1% (w/v) glucose, and 25 $\mu\text{g}/\text{mL}$ chloramphenicol. Bacterial patches were made by resuspending a colony from the aforementioned plates in 100 μL of phosphate-buffered saline (PBS), then depositing 1 μL of that suspension onto both an inducer-free control plate and an inducer LB media plate containing 1.5% (w/v) agar, 1% (w/v) L-arabinose, 0.1% (w/v) glucose, and 25 $\mu\text{g}/\text{mL}$ chloramphenicol using low-retention pipet tips. The bacterial patches were grown at 37°C for 1 day. For each plasmid, two colonies were each used to make three replicate patches on each plate; two inducer and two non-inducer plates were used, leading to twelve induced and twelve non-induced overall replicates for each plasmid (Supplemental Figure 3.S2). GV expression was quantified using a ChemiDoc gel imager (Bio-Rad; Hercules, CA) by measuring the opacity of the patches. Images were processed using ImageJ (NIH; Bethesda, MD). The screen revealed that the V47C mutant expressed the best of the variants.

Large-scale expression and purification of V47C and WT GVs.

GVs were expressed and purified using a protocol similar to that described by Lakshmanan et al.⁷² for the heterologous expression and processing of *Bacillus Megaterium* GVs in *E. coli*.

BL21(DE3) electrically competent *E. coli* cells were transformed with the bARG_{Ser} plasmid with either WT or V47C mutant *gvpA1* and plated. Individual colonies of each variant (WT or V47C) were picked and grown overnight in LB media with 25 $\mu\text{g}/\text{mL}$ chloramphenicol and 1% w/v glucose. The next day, the cultures were saved as glycerol stocks; those glycerol stocks were used to seed all GV-expressing cultures.

GVs were expressed in large batches using 250-mL baffled flasks containing 35 mL LB liquid media with 0.3% w/v glucose, 0.5% w/v L-arabinose, 0.6% w/v glycerol, and 25 $\mu\text{g}/\text{mL}$ chloramphenicol. A 200 μL pipette tip was dug into the appropriate glycerol stock to excavate a small amount (~ 10 μL) of the frozen stock; this frozen stock was then added into 1.5 mL of media in a tube and pipetted up and down. 200 μL of this mixture was used

to seed each of six flasks. Once cells were added to each flask, the flasks were grown at 37°C with 250 rpm shaking for 24 hours.

GV-expressing cultures were poured into 50-mL centrifuge tubes (35 mL of liquid per tube) and centrifuged overnight at 4°C and 350g. The next day, the GV-expressing cells had formed a buoyant layer on top of each tube. The pellet and as much of the media were removed from each tube using an 18G needle and syringe, and then the cells were lysed by resuspending in Solulyse bacterial protein extraction reagent (AMSBIO; Cambridge, MA) totaling 50 mL per variant with 250 µg/mL lysozyme and 10 µg/mL DNase I added. The tubes were rotated at 37°C for 2 hours at 10 rpm, then centrifuged at 4°C and 350g for 8 hours in 50-mL tubes not exceeding 35 mL liquid each. This lysis step was performed a total of four times, but with 25 mL total Solulyse (with lysozyme and DNase I) per variant instead of 50 mL for the subsequent lysis steps. Next, the lysed GV suspension was washed by removing the liquid and pellet from each centrifuged tube and resuspending in 25 mL PBS, then centrifuging the tubes at 4°C and 350g for ~8 hours. This PBS washing step was performed a total of four times as well. After the fourth PBS wash, GVs were unclustered by resuspending them in ~8 mL of 6 M urea in PBS, splitting them into 2-mL tubes with 1 mL volume each, and rotating these tubes at room temperature and 10 rpm for 2 hours. The GVs were then centrifuged for ~6 hours at 4°C and 250g. This unclustering step (removal of liquid with needle, resuspension in 6 M urea in PBS, incubation with rotation, and centrifugation) was also performed a total of four times. Finally, the GVs were dialyzed against 4 L PBS in 6-8 kDa MWCO dialysis tubing a total of four times (i.e., with three buffer changes) to rid them of urea. This resulted in roughly 10 mL of concentrated GVs (V47C optical density at 500 nm [OD₅₀₀] of ~10, WT OD₅₀₀ of ~18). Throughout this process, care was taken not to shake or drop tubes containing GVs to protect them from collapse. Vigorous pipetting of GVs during resuspension steps appears to be tolerated.

Sono-uncaging proof-of-concept experiment.

A 96-well plate was loaded with GVs (V47C [SonoCages] or WT [control]) or PBS mixed with low-melt agarose (LMA) and monobromobimane (mBBBr). The final concentrations

were OD₅₀₀ 3 GVs, 0.5% LMA, and 10 μ M mBBr in 100 μ L total volume per well. Each well was loaded with 60 μ L of concentrated GVs (or PBS) and 40 μ L of a concentrated LMA-mBBr mixture as described below. To allow for US to be performed on only half the wells, the middle four columns of the plate were left empty as a “buffer zone”; the peripheral wells (first and last rows and columns) of the plate were also left empty as they were less accessible to the US transducer. This left two 6x3 regions of wells loaded with sample; the left region was insonated and the right was not.

GV stocks (V47C and WT) were diluted 100x in PBS (10 μ L GV stock into 990 μ L PBS) and their OD₅₀₀ values measured using a cuvette with a 1 cm path length in a Thermo Scientific NanoDrop 2000 spectrophotometer. The approximate stock OD₅₀₀ values were then back-calculated from the diluted OD₅₀₀ values by multiplying by 100. The stock GVs were then diluted to an OD₅₀₀ of 5, and 60 μ L of each appropriate GV variant (V47C, WT, or PBS for a GV-free control) loaded into the corresponding wells of a 96-well plate for a final approximate OD₅₀₀ of 3 in a 100- μ L volume.

Low-melt agarose (LMA) was prepared at a 2% w/v concentration in PBS several days before by adding 2 g of LMA (GoldBio; St. Louis, MO) into 100 mL PBS and microwaving until the agarose dissolved. The LMA solution was stored at 70°C for several days to degas. On the day of the experiment, LMA and mBBr were pre-mixed to reduce the number of pipetting steps when loading the plate. A 1.25% LMA solution containing 25 μ M mBBr was prepared by adding 750 μ L PBS to a 2-mL tube and then pouring 2% LMA solution up to the 2-mL line as 2% LMA is difficult to pipette. The tube was then inverted several times to mix and stored in a heat block at 42°C. 5 μ L of a 50 mM mBBr stock solution was added to the tube and the tube inverted to mix, resulting in a final solution of 1.25% LMA and 25 μ M mBBr. mBBr was purchased from Millipore Sigma (Burlington, MA) as a powder (THIOLYTE, 596105) and reconstituted at a concentration of 13 mg/mL (50 mM) in acetonitrile weeks prior to the experiment; it was aliquoted and stored at 4°C until used. Each well of the plate was loaded with 40 μ L of this LMA-mBBr solution and pipetted up and down 5 times to mix, resulting in the desired final concentrations.

Immediately after each well was loaded, the left half of the plate was placed onto a handheld therapeutic transducer (Richmar Soundcare Plus; Clayton, MO) operating at 3 MHz and coupled with US gel. The plate was moved over the transducer, resulting in the collapse of the GVs in the left half of the wells, which visibly lost their opacity compared to the right-hand wells. Following US collapse, the plate was wiped with a tissue to remove residual US gel and stored in the dark for 1 hour. After 1 hour, the wells of the plate were measured with a Tecan Spark (Tecan Group; Zurich, Switzerland) fluorescence reader with 380/480 nm excitation and emission.

US patterning of GV collapse.

For the US patterning experiments, samples were prepared on individual mylar-bottomed culture dishes. The dishes were made prior to the experiment by removing the glass bottoms from 35 mm dishes (Matsunami Glass USA; Bellingham, WA) and gluing mylar films to the bottoms of the dishes.

On the day of the experiment, the dishes were loaded with GVs, LMA, and mBBr totaling 200 μ L, just enough volume to evenly coat the entire inset well of each dish. Each dish had an identical final concentration as before (OD₅₀₀ 3 GVs [WT or SonoCages], 0.25% LMA, and 10 μ M mBBr), but were loaded in a slightly different manner as before due to the logistical differences between setting up a multiwell assay and individual dishes. In brief, each plate was first loaded with concentrated GVs (WT or SonoCages), then diluted with PBS to 98 μ L. Next, 2 μ L of a 1 mM mBBr solution was added. Finally, 100 μ L of a 0.5% LMA solution in PBS (prepared by pouring 500 μ L 2% LMA stock solution into 1500 μ L PBS in a 2-mL tube and storing at 42°C until ready for use) was added; the mixture was then pipetted up and down, which served both to mix the components and evenly spread them on the mylar. Once the samples were prepared, they were left in the dark for around 15 minutes to solidify, then patterned with US.

After placing the plate on the water surface, we transmitted a focused ultrasound beam onto the plate following pre-designed patterns using a 1024-element matrix array probe

(Vermon, center frequency = 15 MHz, pitch size = 0.3 mm). The probe was submerged in water degassed with a water conditioner (ONDA Corporation; Sunnyvale, CA) and positioned at a 7 mm focal distance from the bottom of the plate. The probe's distance to the plate and its horizontality were confirmed through B-mode imaging. A non-steered focused beam was generated using an 8 x 8 subset of transducer elements from the full 32 x 32 array, enabling the printing of arbitrary patterns based on 25 x 25 two-dimensional binary masks. As for the waveform parameters, the transmit frequency, duty cycle, and the number of cycles were set to 8.9 MHz, 0.67, and 5, respectively. The pulse repetition frequency was 4 kHz. The input voltages applied to the transducer were 25 V for WT GV samples and 20 V for SonoCage samples.

After US patterning, the dishes were imaged with a Zeiss LSM 800 confocal microscope with ZEN Blue. Images were processed with the Fiji package of ImageJ.

3.6 References

- (5) Adams, S. R.; Kao, J. P. Y.; Gryniewicz, G.; Minta, A.; Tsien, R. Y. Biologically Useful Chelators That Release Ca²⁺ upon Illumination. *J. Am. Chem. Soc.* **1988**, *110* (10), 3212–3220. <https://doi.org/10.1021/ja00218a034>.
- (6) Klöcker, N.; Weissenboeck, F. P.; Van Dülmen, M.; Špaček, P.; Hüwel, S.; Rentmeister, A. Photocaged 5' Cap Analogues for Optical Control of mRNA Translation in Cells. *Nat. Chem.* **2022**, *14* (8), 905–913. <https://doi.org/10.1038/s41557-022-00972-7>.
- (7) Kaplan, J. H.; Forbush, B.; Hoffman, J. F. Rapid Photolytic Release of Adenosine 5'-Triphosphate from a Protected Analog: Utilization by the Sodium:Potassium Pump of Human Red Blood Cell Ghosts. *Biochemistry* **1978**, *17* (10), 1929–1935. <https://doi.org/10.1021/bi00603a020>.
- (24) Dutka, P.; Metskas, L. A.; Hurt, R. C.; Salahshoor, H.; Wang, T.-Y.; Malounda, D.; Lu, G. J.; Chou, T.-F.; Shapiro, M. G.; Jensen, G. J. Structure of Anabaena Flos-Aquae Gas Vesicles Revealed by Cryo-ET. *Structure* **2023**, *31* (5), 518-528.e6. <https://doi.org/10.1016/j.str.2023.03.011>.

- (27) Hurt, R. C.; Buss, M. T.; Duan, M.; Wong, K.; You, M. Y.; Sawyer, D. P.; Swift, M. B.; Dutka, P.; Barturen-Larrea, P.; Mittelstein, D. R.; Jin, Z.; Abedi, M. H.; Farhadi, A.; Deshpande, R.; Shapiro, M. G. Genomically Mined Acoustic Reporter Genes for Real-Time in Vivo Monitoring of Tumors and Tumor-Homing Bacteria. *Nat. Biotechnol.* **2023**, *41* (7), 919–931. <https://doi.org/10.1038/s41587-022-01581-y>.
- (36) Jin, Z.; Lakshmanan, A.; Zhang, R.; Tran, T. A.; Rabut, C.; Dutka, P.; Duan, M.; Hurt, R. C.; Malounda, D.; Yao, Y.; Shapiro, M. G. *Ultrasonic Reporters of Calcium for Deep Tissue Imaging of Cellular Signals*; preprint; 2023. <https://doi.org/10.1101/2023.11.09.566364>.
- (48) Tsien, R. Y.; Zucker, R. S. Control of Cytoplasmic Calcium with Photolabile Tetracarboxylate 2-Nitrobenzhydryl Chelators. *Biophys. J.* **1986**, *50* (5), 843–853. [https://doi.org/10.1016/S0006-3495\(86\)83525-1](https://doi.org/10.1016/S0006-3495(86)83525-1).
- (49) Agarwal, H. K.; Janicek, R.; Chi, S.-H.; Perry, J. W.; Niggli, E.; Ellis-Davies, G. C. R. Calcium Uncaging with Visible Light. *J. Am. Chem. Soc.* **2016**, *138* (11), 3687–3693. <https://doi.org/10.1021/jacs.5b11606>.
- (50) Wieboldt, R.; Gee, K. R.; Niu, L.; Ramesh, D.; Carpenter, B. K.; Hess, G. P. Photolabile Precursors of Glutamate: Synthesis, Photochemical Properties, and Activation of Glutamate Receptors on a Microsecond Time Scale. *Proc. Natl. Acad. Sci.* **1994**, *91* (19), 8752–8756. <https://doi.org/10.1073/pnas.91.19.8752>.
- (51) Lee, T. H.; Gee, K. R.; Ellinwood, E. H.; Seidler, F. J. Combining ‘Caged-Dopamine’ Photolysis with Fast-Scan Cyclic Voltammetry to Assess Dopamine Clearance and Release Autoinhibition in Vitro. *J. Neurosci. Methods* **1996**, *67* (2), 221–231. [https://doi.org/10.1016/0165-0270\(96\)00068-4](https://doi.org/10.1016/0165-0270(96)00068-4).
- (52) Asad, N.; McLain, D. E.; Condon, A. F.; Gore, S.; Hampton, S. E.; Vijay, S.; Williams, J. T.; Dore, T. M. Photoactivatable Dopamine and Sulpiride to Explore the Function of Dopaminergic Neurons and Circuits. *ACS Chem. Neurosci.* **2020**, *11* (6), 939–951. <https://doi.org/10.1021/acscchemneuro.9b00675>.
- (53) Ghosh, M.; Ichetovkin, I.; Song, X.; Condeelis, J. S.; Lawrence, D. S. A New Strategy for Caging Proteins Regulated by Kinases. *J. Am. Chem. Soc.* **2002**, *124* (11), 2440–2441. <https://doi.org/10.1021/ja017592l>.

- (54) Chen, X.; Tang, S.; Zheng, J.-S.; Zhao, R.; Wang, Z.-P.; Shao, W.; Chang, H.-N.; Cheng, J.-Y.; Zhao, H.; Liu, L.; Qi, H. Chemical Synthesis of a Two-Photon-Activatable Chemokine and Photon-Guided Lymphocyte Migration in Vivo. *Nat. Commun.* **2015**, *6* (1), 7220. <https://doi.org/10.1038/ncomms8220>.
- (55) Nguyen, D. P.; Mahesh, M.; Elsässer, S. J.; Hancock, S. M.; Uttamapinant, C.; Chin, J. W. Genetic Encoding of Photocaged Cysteine Allows Photoactivation of TEV Protease in Live Mammalian Cells. *J. Am. Chem. Soc.* **2014**, *136* (6), 2240–2243. <https://doi.org/10.1021/ja412191m>.
- (56) Ando, H.; Furuta, T.; Tsien, R. Y.; Okamoto, H. Photo-Mediated Gene Activation Using Caged RNA/DNA in Zebrafish Embryos. *Nat. Genet.* **2001**, *28* (4), 317–325. <https://doi.org/10.1038/ng583>.
- (57) Shestopalov, I. A.; Sinha, S.; Chen, J. K. Light-Controlled Gene Silencing in Zebrafish Embryos. *Nat. Chem. Biol.* **2007**, *3* (10), 650–651. <https://doi.org/10.1038/nchembio.2007.30>.
- (58) Namiki, S.; Arai, T.; Fujimori, K. High-Performance Caged Nitric Oxide: A New Molecular Design, Synthesis, and Photochemical Reaction. *J. Am. Chem. Soc.* **1997**, *119* (16), 3840–3841. <https://doi.org/10.1021/ja962839d>.
- (59) Versaw, B. A.; Zeng, T.; Hu, X.; Robb, M. J. Harnessing the Power of Force: Development of Mechanophores for Molecular Release. *J. Am. Chem. Soc.* **2021**, *143* (51), 21461–21473. <https://doi.org/10.1021/jacs.1c11868>.
- (60) Chen, Y.; Mellot, G.; Van Luijk, D.; Creton, C.; Sijbesma, R. P. Mechanochemical Tools for Polymer Materials. *Chem. Soc. Rev.* **2021**, *50* (6), 4100–4140. <https://doi.org/10.1039/D0CS00940G>.
- (61) Fu, X.; Hu, X. Ultrasound-Controlled Prodrug Activation: Emerging Strategies in Polymer Mechanochemistry and Sonodynamic Therapy. *ACS Appl. Bio Mater.* **2024**, *7* (12), 8040–8058. <https://doi.org/10.1021/acsabm.4c00150>.
- (62) Martínez, R. F.; Cravotto, G.; Cintas, P. Organic Sonochemistry: A Chemist's Timely Perspective on Mechanisms and Reactivity. *J. Org. Chem.* **2021**, *86* (20), 13833–13856. <https://doi.org/10.1021/acs.joc.1c00805>.

- (63) Choi, V.; Rajora, M. A.; Zheng, G. Activating Drugs with Sound: Mechanisms Behind Sonodynamic Therapy and the Role of Nanomedicine. *Bioconjug. Chem.* **2020**, *31* (4), 967–989. <https://doi.org/10.1021/acs.bioconjchem.0c00029>.
- (64) Suslick, K. S. Sonochemistry. *Science* **1990**, *247* (4949), 1439–1445. <https://doi.org/10.1126/science.247.4949.1439>.
- (65) Mitragotri, S. Healing Sound: The Use of Ultrasound in Drug Delivery and Other Therapeutic Applications. *Nat. Rev. Drug Discov.* **2005**, *4* (3), 255–260. <https://doi.org/10.1038/nrd1662>.
- (66) Nyström, N. N.; Jin, Z.; Bennett, M. E.; Zhang, R.; Swift, M. B.; Shapiro, M. G. *Multiplexed Ultrasound Imaging of Gene Expression*; preprint; November 3, 2024. <https://doi.org/10.1101/2024.10.30.621148>.
- (67) Schrunk, E.; Dutka, P.; Hurt, R. C.; Wu, D.; Shapiro, M. G. Bioorthogonal Labeling Enables In Situ Fluorescence Imaging of Expressed Gas Vesicle Nanostructures. *Bioconjug. Chem.* **2024**, *35* (3), 333–339. <https://doi.org/10.1021/acs.bioconjchem.3c00518>.
- (68) Kosower, N. S.; Kosower, E. M.; Newton, G. L.; Ranney, H. M. Bimane Fluorescent Labels: Labeling of Normal Human Red Cells under Physiological Conditions. *Proc. Natl. Acad. Sci.* **1979**, *76* (7), 3382–3386. <https://doi.org/10.1073/pnas.76.7.3382>.
- (69) Liu, C. C.; Schultz, P. G. Adding New Chemistries to the Genetic Code. *Annu. Rev. Biochem.* **2010**, *79* (1), 413–444. <https://doi.org/10.1146/annurev.biochem.052308.105824>.
- (70) Birch-Price, Z.; Hardy, F. J.; Lister, T. M.; Kohn, A. R.; Green, A. P. Noncanonical Amino Acids in Biocatalysis. *Chem. Rev.* **2024**, *124* (14), 8740–8786. <https://doi.org/10.1021/acs.chemrev.4c00120>.
- (71) Hurt, R. C.; Jin, Z.; Soufi, M.; Wong, K. K.; Sawyer, D. P.; Shen, H. K.; Dutka, P.; Deshpande, R.; Zhang, R.; Mittelstein, D. R.; Shapiro, M. G. Directed Evolution of Acoustic Reporter Genes Using High-Throughput Acoustic Screening. *ACS Synth. Biol.* **2024**, *13* (7), 2215–2226. <https://doi.org/10.1021/acssynbio.4c00283>.
- (72) Lakshmanan, A.; Lu, G. J.; Farhadi, A.; Nety, S. P.; Kunth, M.; Lee-Gosselin, A.; Maresca, D.; Bourdeau, R. W.; Yin, M.; Yan, J.; Witte, C.; Malounda, D.; Foster, F.

S.; Schröder, L.; Shapiro, M. G. Preparation of Biogenic Gas Vesicle Nanostructures for Use as Contrast Agents for Ultrasound and MRI. *Nat. Protoc.* **2017**, *12* (10), 2050–2080. <https://doi.org/10.1038/nprot.2017.081>.

3.7 Supporting information

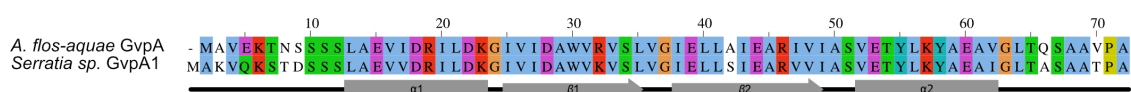


Figure 3.S1: Sequence alignment for *Anabaena flos-aquae* gvpA and *Serratia* sp. 39006 gvpA1. The two genes have an identity score of 80.6% (58 of 72 amino acids) and a similarity score of 91.7% (66 of 72 amino acids). Colored amino acids represent pairs of amino acids with similar or identical side chains: blue for hydrophobic groups, purple for negatively charged groups, green for polar uncharged groups, red for positively charged groups, orange for glycine, teal for aromatic groups (tyrosine and histidine), and yellow for proline.

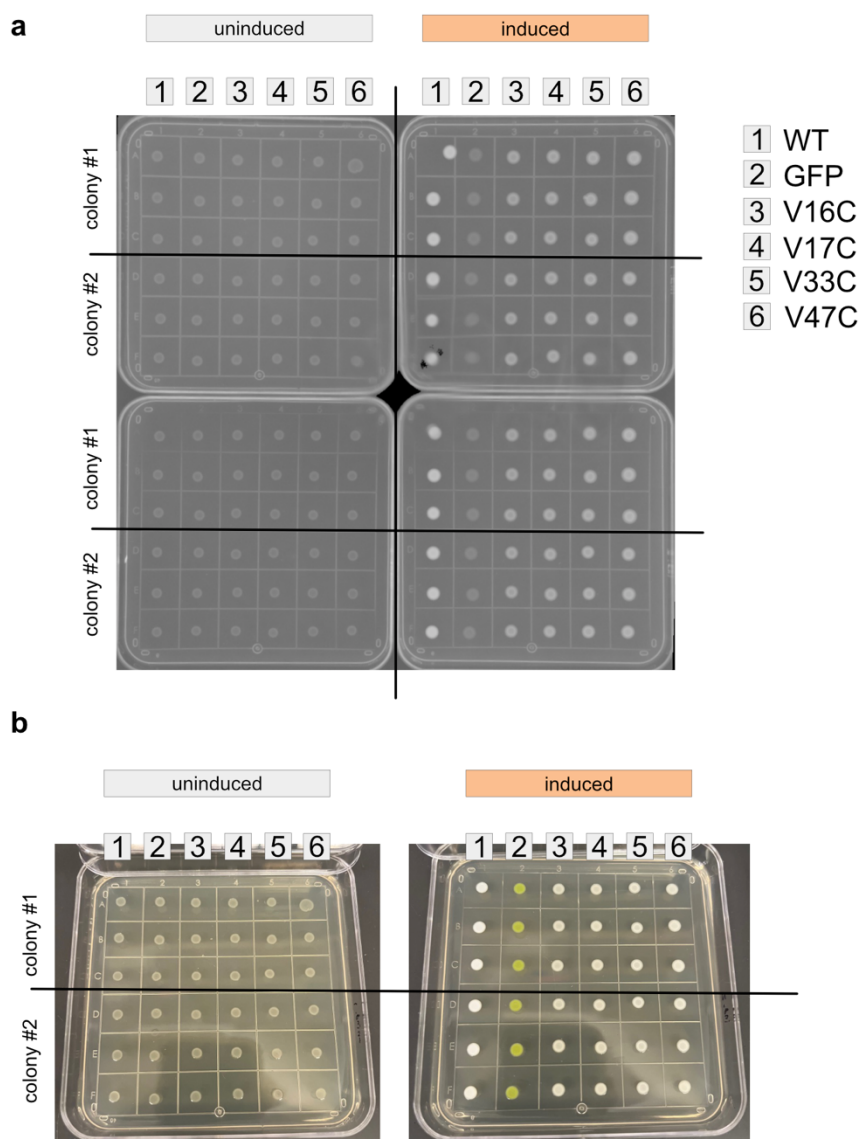


Figure 3.S2: SonoCage candidate screen on patch plates. (a) Absorbance image of all four plates (two uninduced plates on left, two induced plates on right) taken 1 day after plating. On each plate, each column (labeled 1-6) denotes a different mutant or control. In each column, the first three rows are technical replicates made from the same original colony, and the next three rows are technical replicates made from another colony. (b) Phone camera image of two plates (one uninduced, one induced) taken 1 day after plating.

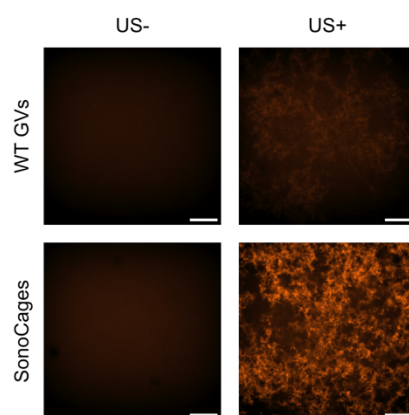


Figure 3.S3: Confocal microscopy images of mBBr fluorescence in WT GV and SonoCage samples prepared in PBS on a glass-bottomed dish. Fluorescence is highest in the US-treated SonoCage samples due to the mBBr-thiol reaction. The slight increase in fluorescence post US in the WT GV samples can be attributed to a drop in opacity (and increase in brightness) concomitant with GV collapse.

CONCLUSION, FUTURE DIRECTIONS, AND FINAL THOUGHTS

In this work, I discussed the development of GVs with exterior- and interior-facing mutations to cysteine whose mutations were discovered through the same screen but that functionally affected the GVs in vastly different ways. The results from those projects naturally lead to follow-up questions and research directions. In the next few pages, I will briefly discuss some of the research aims that I believe proceed from and build off our above findings.

4.1 Incorporation of non-canonical amino acids into GVs

In the original conception of this project, I hoped to incorporate several non-canonical amino acids (ncAAs) into GVs, especially for the purpose of sono-uncaging. Cysteine was meant to be a “trial run” amino acid as it is arguably the most chemically unique of the natural amino acids, which can be incorporated into proteins using the endogenous translation machinery under normal media conditions. While the ease of using cysteine did lead to useful results and undoubtedly involved less optimization, troubleshooting, and cell health issues compared to using ncAAs, I still believe that the functionalization of GVs with ncAAs is a natural next step in this experimental progression.

A vast number of ncAAs have been described in literature.^{69,70,73,74} Their unique side chains vary widely in form, ranging from slight modifications of natural side chains to chemical groups infrequently or not at all found in nature (like the azide and alkyne groups of azidohomoalanine^{75,76} and homopropargylglycine^{77,78}, respectively). Our hope is that any ncAA with a reactive, sufficiently hydrophobic (so that it can stably exist in the air-filled GV interior) side chain of choice can be sono-uncaged. While ncAA incorporation schemes vary slightly, the general workflow would involve a screen of GvpA1 similar to that discussed in Chapters 2 and 3, but with an appropriate codon (in many cases the amber stop codon) and the desired ncAA present in a sufficiently formulated growth medium. The resulting GV-expressing mutations could then be sequenced and cross-referenced against the hypothesized

interior-facing sites from Chapter 3, leading immediately to top sono-uncaging candidates. Side chains that bear potentially reactive groups do mainly appear to be polar and likely hydrophilic; however, side chains with reactive nonpolar groups like alkenes and alkynes⁷⁹ have been described. Given that we were able to cage cysteine, perhaps ncAAs with other groups like isothiocyanate⁸⁰ and selenol⁸¹ (as well as the naturally occurring amino acid selenocysteine⁸²) are possible as well.

4.2 GVs with exterior disulfide bonds and multiple mutations to GvpA1

Our results (see Figure 3.2) indicate that there are many exterior-facing cysteine-tolerant sites scattered throughout much of GvpA1, not just its C-terminus. It could be possible to create a GvpA1 with external-facing cysteines that are close enough to the cysteines on adjacent GvpA1 molecules that disulfide bonds can form under proper conditions. These disulfide-crosslinked “stapled” GVs would likely exhibit significantly different acoustic properties than WT GVs due to their more rigidly connected shells. These acoustic effects would probably be able to be reversed under reducing conditions, allowing the GVs to serve as acoustic redox sensors, although the original disulfide crosslinking step might only be possible if the redox environment within the cell is sufficiently oxidative. This approach would involve the simultaneous mutation of multiple amino acids in GvpA1 to cysteine to allow each GvpA1 to bond with multiple neighbors.

It is also worth noting that we found multiple potential interior-facing cysteine mutants in our mutant screen to discover sono-uncaging candidates. We used the best-expressing mutant, V47C, as the basis for SonoCages, but other mutants also expressed GVs to lesser degrees. If any of the other sites from the screen can also undergo sono-uncaging, it could be possible to engineer SonoCages with two or more simultaneous interior-facing mutations to cysteine in GvpA1, thereby increasing the concentration of uncaged thiol. While this approach will likely decrease GV expression levels, it could be used if higher concentrations of cysteine are necessary; optimization of expression conditions and scale-up of GV production could overcome the issue of lowered expression level.

4.3 Expressing chimeric GVs in HEK 293T cells with a WT/modified GvpA cocktail

In Chapter 2, we demonstrated the expression of chimeric GVs in HEK 293T cells through the delivery of a mixture of wild-type (WT) and altered GvpA. This approach has potentially important implications for future GV work as it shows that even when a modified GvpA abrogates GV formation, it is possible to successfully incorporate some of that modified GvpA into a GV structure by co-transfecting it alongside WT GvpA. GvpA has come to be known as very intolerant of fusions and modifications, but perhaps with the right ratio of engineered to WT GvpA, a chimeric GV with a small proportion of altered subunits can still be expressed. This insight potentially revives the concept of direct fusions (such as GFP or HaloTag⁸³) to GvpA and grants some feasibility to the idea of “loading” enzymes into GV interiors.

4.4 Final thoughts

It has been a great journey working on these projects in this lab, and I could not have done it without Mikhail’s guidance, insights, and patience. I cannot thank him enough. I also thank you, reader, for making it all the way down here. I am sure reading through all those pages was quite the journey as well.

I joined the lab because I believed GVs were an amazing, elegant solution to the problems presented by the opacity of tissue. Today, even though I have complained countless times about my research not working, my faith in GVs and their applications is even stronger than before. It was a pleasure working with these tiny structures, and I now know them well—you could even say I know them inside and out.

4.5 References

- (69) Liu, C. C.; Schultz, P. G. Adding New Chemistries to the Genetic Code. *Annu. Rev. Biochem.* **2010**, 79 (1), 413–444.
<https://doi.org/10.1146/annurev.biochem.052308.105824>.

- (70) Birch-Price, Z.; Hardy, F. J.; Lister, T. M.; Kohn, A. R.; Green, A. P. Noncanonical Amino Acids in Biocatalysis. *Chem. Rev.* **2024**, *124* (14), 8740–8786. <https://doi.org/10.1021/acs.chemrev.4c00120>.
- (73) Iskandar, S. E.; Haberman, V. A.; Bowers, A. A. Expanding the Chemical Diversity of Genetically Encoded Libraries. *ACS Comb. Sci.* **2020**, *22* (12), 712–733. <https://doi.org/10.1021/acscombsci.0c00179>.
- (74) Brouwer, B.; Della-Felice, F.; Illies, J. H.; Iglesias-Moncayo, E.; Roelfes, G.; Drienovská, I. Noncanonical Amino Acids: Bringing New-to-Nature Functionalities to Biocatalysis. *Chem. Rev.* **2024**, *124* (19), 10877–10923. <https://doi.org/10.1021/acs.chemrev.4c00136>.
- (75) Dieterich, D. C.; Link, A. J.; Graumann, J.; Tirrell, D. A.; Schuman, E. M. Selective Identification of Newly Synthesized Proteins in Mammalian Cells Using Bioorthogonal Noncanonical Amino Acid Tagging (BONCAT). *Proc. Natl. Acad. Sci.* **2006**, *103* (25), 9482–9487. <https://doi.org/10.1073/pnas.0601637103>.
- (76) Link, A. J.; Tirrell, D. A. Cell Surface Labeling of *Escherichia coli* via Copper(I)-Catalyzed [3+2] Cycloaddition. *J. Am. Chem. Soc.* **2003**, *125* (37), 11164–11165. <https://doi.org/10.1021/ja036765z>.
- (77) Ngo, J. T.; Tirrell, D. A. Noncanonical Amino Acids in the Interrogation of Cellular Protein Synthesis. *Acc. Chem. Res.* **2011**, *44* (9), 677–685. <https://doi.org/10.1021/ar200144y>.
- (78) Prescher, J. A.; Bertozzi, C. R. Chemistry in Living Systems. *Nat. Chem. Biol.* **2005**, *1* (1), 13–21. <https://doi.org/10.1038/nchembio0605-13>.
- (79) Van Hest, J. C. M.; Kiick, K. L.; Tirrell, D. A. Efficient Incorporation of Unsaturated Methionine Analogues into Proteins in Vivo. *J. Am. Chem. Soc.* **2000**, *122* (7), 1282–1288. <https://doi.org/10.1021/ja992749j>.
- (80) Li, J. C.; Nasertorabi, F.; Xuan, W.; Han, G. W.; Stevens, R. C.; Schultz, P. G. A Single Reactive Noncanonical Amino Acid Is Able to Dramatically Stabilize Protein Structure. *ACS Chem. Biol.* **2019**, *14* (6), 1150–1153. <https://doi.org/10.1021/acscchembio.9b00002>.

- (81) An, X.; Chen, C.; Wang, T.; Huang, A.; Zhang, D.; Han, M.; Wang, J. Genetic Incorporation of Selenotyrosine Significantly Improves Enzymatic Activity of *Agrobacterium Radiobacter* Phosphotriesterase. *ChemBioChem* **2021**, *22* (15), 2535–2539. <https://doi.org/10.1002/cbic.202000460>.
- (82) Chung, C. Z.; Krahn, N. The Selenocysteine Toolbox: A Guide to Studying the 21st Amino Acid. *Arch. Biochem. Biophys.* **2022**, *730*, 109421. <https://doi.org/10.1016/j.abb.2022.109421>.
- (83) Los, G. V.; Encell, L. P.; McDougall, M. G.; Hartzell, D. D.; Karassina, N.; Zimprich, C.; Wood, M. G.; Learish, R.; Ohana, R. F.; Urh, M.; Simpson, D.; Mendez, J.; Zimmerman, K.; Otto, P.; Vidugiris, G.; Zhu, J.; Darzins, A.; Klaubert, D. H.; Bulleit, R. F.; Wood, K. V. HaloTag: A Novel Protein Labeling Technology for Cell Imaging and Protein Analysis. *ACS Chem. Biol.* **2008**, *3* (6), 373–382. <https://doi.org/10.1021/cb800025k>.

ALL REFERENCES

- (1) Tsien, R. Y. The Green Fluorescent Protein. *Annu. Rev. Biochem.* **1998**, *67* (1), 509–544. <https://doi.org/10.1146/annurev.biochem.67.1.509>.
- (2) Deisseroth, K. Optogenetics: 10 Years of Microbial Opsins in Neuroscience. *Nat. Neurosci.* **2015**, *18* (9), 1213–1225. <https://doi.org/10.1038/nn.4091>.
- (3) Pan, Z.-H.; Lu, Q.; Bi, A.; Dizhoor, A. M.; Abrams, G. W. Optogenetic Approaches to Restoring Vision. *Annu. Rev. Vis. Sci.* **2015**, *1* (1), 185–210. <https://doi.org/10.1146/annurev-vision-082114-035532>.
- (4) Ellis-Davies, G. C. R. Caged Compounds: Photorelease Technology for Control of Cellular Chemistry and Physiology. *Nat. Methods* **2007**, *4* (8), 619–628. <https://doi.org/10.1038/nmeth1072>.
- (5) Adams, S. R.; Kao, J. P. Y.; Grynkiewicz, G.; Minta, A.; Tsien, R. Y. Biologically Useful Chelators That Release Ca²⁺ upon Illumination. *J. Am. Chem. Soc.* **1988**, *110* (10), 3212–3220. <https://doi.org/10.1021/ja00218a034>.
- (6) Klöcker, N.; Weissenboeck, F. P.; Van Dülmen, M.; Špaček, P.; Hüwel, S.; Rentmeister, A. Photocaged 5' Cap Analogues for Optical Control of mRNA Translation in Cells. *Nat. Chem.* **2022**, *14* (8), 905–913. <https://doi.org/10.1038/s41557-022-00972-7>.
- (7) Kaplan, J. H.; Forbush, B.; Hoffman, J. F. Rapid Photolytic Release of Adenosine 5'-Triphosphate from a Protected Analog: Utilization by the Sodium:Potassium Pump of Human Red Blood Cell Ghosts. *Biochemistry* **1978**, *17* (10), 1929–1935. <https://doi.org/10.1021/bi00603a020>.
- (8) Piraner, D. I.; Farhadi, A.; Davis, H. C.; Wu, D.; Maresca, D.; Szablowski, J. O.; Shapiro, M. G. Going Deeper: Biomolecular Tools for Acoustic and Magnetic Imaging and Control of Cellular Function. *Biochemistry* **2017**, *56* (39), 5202–5209. <https://doi.org/10.1021/acs.biochem.7b00443>.
- (9) Rosenberg, S. A.; Restifo, N. P.; Yang, J. C.; Morgan, R. A.; Dudley, M. E. Adoptive Cell Transfer: A Clinical Path to Effective Cancer Immunotherapy. *Nat. Rev. Cancer* **2008**, *8* (4), 299–308. <https://doi.org/10.1038/nrc2355>.

- (10) Sterner, R. C.; Sterner, R. M. CAR-T Cell Therapy: Current Limitations and Potential Strategies. *Blood Cancer J.* **2021**, *11* (4), 69. <https://doi.org/10.1038/s41408-021-00459-7>.
- (11) Riglar, D. T.; Silver, P. A. Engineering Bacteria for Diagnostic and Therapeutic Applications. *Nat. Rev. Microbiol.* **2018**, *16* (4), 214–225. <https://doi.org/10.1038/nrmicro.2017.172>.
- (12) Charbonneau, M. R.; Isabella, V. M.; Li, N.; Kurtz, C. B. Developing a New Class of Engineered Live Bacterial Therapeutics to Treat Human Diseases. *Nat. Commun.* **2020**, *11* (1), 1738. <https://doi.org/10.1038/s41467-020-15508-1>.
- (13) Luker, K. E.; Luker, G. D. Bioluminescence Imaging of Reporter Mice for Studies of Infection and Inflammation. *Antiviral Res.* **2010**, *86* (1), 93–100. <https://doi.org/10.1016/j.antiviral.2010.02.002>.
- (14) Liu, S.; Su, Y.; Lin, M. Z.; Ronald, J. A. Brightening up Biology: Advances in Luciferase Systems for *in Vivo* Imaging. *ACS Chem. Biol.* **2021**, *16* (12), 2707–2718. <https://doi.org/10.1021/acscchembio.1c00549>.
- (15) Benard, E. L.; Van Der Sar, A. M.; Ellett, F.; Lieschke, G. J.; Spaink, H. P.; Meijer, A. H. Infection of Zebrafish Embryos with Intracellular Bacterial Pathogens. *J. Vis. Exp.* **2012**, No. 61, 3781. <https://doi.org/10.3791/3781>.
- (16) Meijer, A. H.; Van Der Vaart, M.; Spaink, H. P. Real-Time Imaging and Genetic Dissection of Host-Microbe Interactions in Zebrafish: Dissecting Host-Microbe Interactions in Zebrafish. *Cell. Microbiol.* **2014**, *16* (1), 39–49. <https://doi.org/10.1111/cmi.12236>.
- (17) Levraud, J.-P.; Palha, N.; Langevin, C.; Boudinot, P. Through the Looking Glass: Witnessing Host–Virus Interplay in Zebrafish. *Trends Microbiol.* **2014**, *22* (9), 490–497. <https://doi.org/10.1016/j.tim.2014.04.014>.
- (18) Secklehner, J.; Lo Celso, C.; Carlin, L. M. Intravital Microscopy in Historic and Contemporary Immunology. *Immunol. Cell Biol.* **2017**, *95* (6), 506–513. <https://doi.org/10.1038/icb.2017.25>.
- (19) Choe, K.; Hontani, Y.; Wang, T.; Hebert, E.; Ouzounov, D. G.; Lai, K.; Singh, A.; Béguelin, W.; Melnick, A. M.; Xu, C. Intravital Three-Photon Microscopy Allows

- Visualization over the Entire Depth of Mouse Lymph Nodes. *Nat. Immunol.* **2022**, *23* (2), 330–340. <https://doi.org/10.1038/s41590-021-01101-1>.
- (20) Ouzounov, D. G.; Wang, T.; Wang, M.; Feng, D. D.; Horton, N. G.; Cruz-Hernández, J. C.; Cheng, Y.-T.; Reimer, J.; Tolia, A. S.; Nishimura, N.; Xu, C. In Vivo Three-Photon Imaging of Activity of GCaMP6-Labeled Neurons Deep in Intact Mouse Brain. *Nat. Methods* **2017**, *14* (4), 388–390. <https://doi.org/10.1038/nmeth.4183>.
- (21) Farhadi, A.; Ho, G. H.; Sawyer, D. P.; Bourdeau, R. W.; Shapiro, M. G. Ultrasound Imaging of Gene Expression in Mammalian Cells. *Science* **2019**, *365* (6460), 1469–1475. <https://doi.org/10.1126/science.aax4804>.
- (22) Maresca, D.; Lakshmanan, A.; Abedi, M.; Bar-Zion, A.; Farhadi, A.; Lu, G. J.; Szablowski, J. O.; Wu, D.; Yoo, S.; Shapiro, M. G. Biomolecular Ultrasound and Sonogenetics. *Annu. Rev. Chem. Biomol. Eng.* **2018**, *9* (1), 229–252. <https://doi.org/10.1146/annurev-chembioeng-060817-084034>.
- (23) Ibsen, S.; Tong, A.; Schutt, C.; Esener, S.; Chalasani, S. H. Sonogenetics Is a Non-Invasive Approach to Activating Neurons in *Caenorhabditis Elegans*. *Nat. Commun.* **2015**, *6* (1), 8264. <https://doi.org/10.1038/ncomms9264>.
- (24) Dutka, P.; Metskas, L. A.; Hurt, R. C.; Salahshoor, H.; Wang, T.-Y.; Malounda, D.; Lu, G. J.; Chou, T.-F.; Shapiro, M. G.; Jensen, G. J. Structure of *Anabaena Flos-Aquae* Gas Vesicles Revealed by Cryo-ET. *Structure* **2023**, *31* (5), 518–528.e6. <https://doi.org/10.1016/j.str.2023.03.011>.
- (25) Walsby, A. E. Gas Vesicles. *Microbiol. Rev.* **1994**, *58* (1), 94–144. <https://doi.org/10.1128/mr.58.1.94-144.1994>.
- (26) Bourdeau, R. W.; Lee-Gosselin, A.; Lakshmanan, A.; Farhadi, A.; Kumar, S. R.; Nety, S. P.; Shapiro, M. G. Acoustic Reporter Genes for Noninvasive Imaging of Microorganisms in Mammalian Hosts. *Nature* **2018**, *553* (7686), 86–90. <https://doi.org/10.1038/nature25021>.
- (27) Hurt, R. C.; Buss, M. T.; Duan, M.; Wong, K.; You, M. Y.; Sawyer, D. P.; Swift, M. B.; Dutka, P.; Barturen-Larrea, P.; Mittelstein, D. R.; Jin, Z.; Abedi, M. H.; Farhadi, A.; Deshpande, R.; Shapiro, M. G. Genomically Mined Acoustic Reporter Genes for Real-

- Time in Vivo Monitoring of Tumors and Tumor-Homing Bacteria. *Nat. Biotechnol.* **2023**, *41* (7), 919–931. <https://doi.org/10.1038/s41587-022-01581-y>.
- (28) Lakshmanan, A.; Jin, Z.; Nety, S. P.; Sawyer, D. P.; Lee-Gosselin, A.; Malounda, D.; Swift, M. B.; Maresca, D.; Shapiro, M. G. Acoustic Biosensors for Ultrasound Imaging of Enzyme Activity. *Nat. Chem. Biol.* **2020**, *16* (9), 988–996. <https://doi.org/10.1038/s41589-020-0591-0>.
- (29) Bar-Zion, A.; Nourmahnad, A.; Mittelstein, D. R.; Shivaiei, S.; Yoo, S.; Buss, M. T.; Hurt, R. C.; Malounda, D.; Abedi, M. H.; Lee-Gosselin, A.; Swift, M. B.; Maresca, D.; Shapiro, M. G. Acoustically Triggered Mechanotherapy Using Genetically Encoded Gas Vesicles. *Nat. Nanotechnol.* **2021**, *16* (12), 1403–1412. <https://doi.org/10.1038/s41565-021-00971-8>.
- (30) Wu, D.; Baresch, D.; Cook, C.; Ma, Z.; Duan, M.; Malounda, D.; Maresca, D.; Abundo, M. P.; Lee, J.; Shivaiei, S.; Mittelstein, D. R.; Qiu, T.; Fischer, P.; Shapiro, M. G. Biomolecular Actuators for Genetically Selective Acoustic Manipulation of Cells. *Sci. Adv.* **2023**, *9* (8), eadd9186. <https://doi.org/10.1126/sciadv.add9186>.
- (31) Belenky, M.; Meyers, R.; Herzfeld, J. Subunit Structure of Gas Vesicles: A MALDI-TOF Mass Spectrometry Study. *Biophys. J.* **2004**, *86* (1), 499–505. [https://doi.org/10.1016/S0006-3495\(04\)74128-4](https://doi.org/10.1016/S0006-3495(04)74128-4).
- (32) Sigmund, F.; Berezin, O.; Beliakova, S.; Magerl, B.; Drawitsch, M.; Piovesan, A.; Gonçalves, F.; Bodea, S.-V.; Winkler, S.; Bousraou, Z.; Grosshauser, M.; Samara, E.; Pujol-Martí, J.; Schädler, S.; So, C.; Irsen, S.; Walch, A.; Kofler, F.; Piraud, M.; Kornfeld, J.; Briggman, K.; Westmeyer, G. G. Genetically Encoded Barcodes for Correlative Volume Electron Microscopy. *Nat. Biotechnol.* **2023**. <https://doi.org/10.1038/s41587-023-01713-y>.
- (33) Mohsen, M. O.; Bachmann, M. F. Virus-like Particle Vaccinology, from Bench to Bedside. *Cell. Mol. Immunol.* **2022**, *19* (9), 993–1011. <https://doi.org/10.1038/s41423-022-00897-8>.
- (34) Edwardson, T. G. W.; Mori, T.; Hilvert, D. Rational Engineering of a Designed Protein Cage for siRNA Delivery. *J. Am. Chem. Soc.* **2018**, *140* (33), 10439–10442. <https://doi.org/10.1021/jacs.8b06442>.

- (35) Ling, B.; Lee, J.; Maresca, D.; Lee-Gosselin, A.; Malounda, D.; Swift, M. B.; Shapiro, M. G. Biomolecular Ultrasound Imaging of Phagolysosomal Function. *ACS Nano* **2020**, *14* (9), 12210–12221. <https://doi.org/10.1021/acsnano.0c05912>.
- (36) Jin, Z.; Lakshmanan, A.; Zhang, R.; Tran, T. A.; Rabut, C.; Dutka, P.; Duan, M.; Hurt, R. C.; Malounda, D.; Yao, Y.; Shapiro, M. G. *Ultrasonic Reporters of Calcium for Deep Tissue Imaging of Cellular Signals*; preprint; 2023. <https://doi.org/10.1101/2023.11.09.566364>.
- (37) Griffin, B. A.; Adams, S. R.; Tsien, R. Y. Specific Covalent Labeling of Recombinant Protein Molecules Inside Live Cells. *Science* **1998**, *281* (5374), 269–272. <https://doi.org/10.1126/science.281.5374.269>.
- (38) Adams, S. R.; Campbell, R. E.; Gross, L. A.; Martin, B. R.; Walkup, G. K.; Yao, Y.; Llopis, J.; Tsien, R. Y. New Biarsenical Ligands and Tetracysteine Motifs for Protein Labeling in Vitro and in Vivo: Synthesis and Biological Applications. *J. Am. Chem. Soc.* **2002**, *124* (21), 6063–6076. <https://doi.org/10.1021/ja017687n>.
- (39) Martin, B. R.; Giepmans, B. N. G.; Adams, S. R.; Tsien, R. Y. Mammalian Cell-Based Optimization of the Biarsenical-Binding Tetracysteine Motif for Improved Fluorescence and Affinity. *Nat. Biotechnol.* **2005**, *23* (10), 1308–1314. <https://doi.org/10.1038/nbt1136>.
- (40) Hoffmann, C.; Gaietta, G.; Zürn, A.; Adams, S. R.; Terrillon, S.; Ellisman, M. H.; Tsien, R. Y.; Lohse, M. J. Fluorescent Labeling of Tetracysteine-Tagged Proteins in Intact Cells. *Nat. Protoc.* **2010**, *5* (10), 1666–1677. <https://doi.org/10.1038/nprot.2010.129>.
- (41) Huber, S. T.; Terwiel, D.; Evers, W. H.; Maresca, D.; Jakobi, A. J. Cryo-EM Structure of Gas Vesicles for Buoyancy-Controlled Motility. *Cell* **2023**, *186* (5), 975–986.e13. <https://doi.org/10.1016/j.cell.2023.01.041>.
- (42) Lakshmanan, A.; Farhadi, A.; Nety, S. P.; Lee-Gosselin, A.; Bourdeau, R. W.; Maresca, D.; Shapiro, M. G. Molecular Engineering of Acoustic Protein Nanostructures. *ACS Nano* **2016**, *10* (8), 7314–7322. <https://doi.org/10.1021/acsnano.6b03364>.
- (43) Lu, G. J.; Chou, L.; Malounda, D.; Patel, A. K.; Welsbie, D. S.; Chao, D. L.; Ramalingam, T.; Shapiro, M. G. Genetically Encodable Contrast Agents for Optical

- Coherence Tomography. *ACS Nano* **2020**, *14* (7), 7823–7831. <https://doi.org/10.1021/acsnano.9b08432>.
- (44) Farhadi, A.; Bedrossian, M.; Lee, J.; Ho, G. H.; Shapiro, M. G.; Nadeau, J. L. Genetically Encoded Phase Contrast Agents for Digital Holographic Microscopy. *Nano Lett.* **2020**, *20* (11), 8127–8134. <https://doi.org/10.1021/acs.nanolett.0c03159>.
- (45) Zlatkine, P.; Mehul, B.; Magee, A. I. Retargeting of Cytosolic Proteins to the Plasma Membrane by the Lck Protein Tyrosine Kinase Dual Acylation Motif. *J. Cell Sci.* **1997**, *110* (5), 673–679. <https://doi.org/10.1242/jcs.110.5.673>.
- (46) Pelletier, J.; Sonenberg, N. Internal Initiation of Translation of Eukaryotic mRNA Directed by a Sequence Derived from Poliovirus RNA. *Nature* **1988**, *334* (6180), 320–325. <https://doi.org/10.1038/334320a0>.
- (47) Duan, M.; Dev, I.; Lu, A.; Ayrapetyan, G.; You, M. Y.; Shapiro, M. G. SEMPER: Stoichiometric Expression of mRNA Polycistrons by Eukaryotic Ribosomes for Compact, Ratio-Tunable Multi-Gene Expression. *Cell Syst.* **2024**, *15* (7), 597–609.e4. <https://doi.org/10.1016/j.cels.2024.06.001>.
- (48) Tsien, R. Y.; Zucker, R. S. Control of Cytoplasmic Calcium with Photolabile Tetracarboxylate 2-Nitrobenzhydrol Chelators. *Biophys. J.* **1986**, *50* (5), 843–853. [https://doi.org/10.1016/S0006-3495\(86\)83525-1](https://doi.org/10.1016/S0006-3495(86)83525-1).
- (49) Agarwal, H. K.; Janicek, R.; Chi, S.-H.; Perry, J. W.; Niggli, E.; Ellis-Davies, G. C. R. Calcium Uncaging with Visible Light. *J. Am. Chem. Soc.* **2016**, *138* (11), 3687–3693. <https://doi.org/10.1021/jacs.5b11606>.
- (50) Wieboldt, R.; Gee, K. R.; Niu, L.; Ramesh, D.; Carpenter, B. K.; Hess, G. P. Photolabile Precursors of Glutamate: Synthesis, Photochemical Properties, and Activation of Glutamate Receptors on a Microsecond Time Scale. *Proc. Natl. Acad. Sci.* **1994**, *91* (19), 8752–8756. <https://doi.org/10.1073/pnas.91.19.8752>.
- (51) Lee, T. H.; Gee, K. R.; Ellinwood, E. H.; Seidler, F. J. Combining ‘Caged-Dopamine’ Photolysis with Fast-Scan Cyclic Voltammetry to Assess Dopamine Clearance and Release Autoinhibition in Vitro. *J. Neurosci. Methods* **1996**, *67* (2), 221–231. [https://doi.org/10.1016/0165-0270\(96\)00068-4](https://doi.org/10.1016/0165-0270(96)00068-4).

- (52) Asad, N.; McLain, D. E.; Condon, A. F.; Gore, S.; Hampton, S. E.; Vijay, S.; Williams, J. T.; Dore, T. M. Photoactivatable Dopamine and Sulpiride to Explore the Function of Dopaminergic Neurons and Circuits. *ACS Chem. Neurosci.* **2020**, *11* (6), 939–951. <https://doi.org/10.1021/acchemneuro.9b00675>.
- (53) Ghosh, M.; Ichetovkin, I.; Song, X.; Condeelis, J. S.; Lawrence, D. S. A New Strategy for Caging Proteins Regulated by Kinases. *J. Am. Chem. Soc.* **2002**, *124* (11), 2440–2441. <https://doi.org/10.1021/ja017592l>.
- (54) Chen, X.; Tang, S.; Zheng, J.-S.; Zhao, R.; Wang, Z.-P.; Shao, W.; Chang, H.-N.; Cheng, J.-Y.; Zhao, H.; Liu, L.; Qi, H. Chemical Synthesis of a Two-Photon-Activatable Chemokine and Photon-Guided Lymphocyte Migration in Vivo. *Nat. Commun.* **2015**, *6* (1), 7220. <https://doi.org/10.1038/ncomms8220>.
- (55) Nguyen, D. P.; Mahesh, M.; Elsässer, S. J.; Hancock, S. M.; Uttamapinant, C.; Chin, J. W. Genetic Encoding of Photocaged Cysteine Allows Photoactivation of TEV Protease in Live Mammalian Cells. *J. Am. Chem. Soc.* **2014**, *136* (6), 2240–2243. <https://doi.org/10.1021/ja412191m>.
- (56) Ando, H.; Furuta, T.; Tsien, R. Y.; Okamoto, H. Photo-Mediated Gene Activation Using Caged RNA/DNA in Zebrafish Embryos. *Nat. Genet.* **2001**, *28* (4), 317–325. <https://doi.org/10.1038/ng583>.
- (57) Shestopalov, I. A.; Sinha, S.; Chen, J. K. Light-Controlled Gene Silencing in Zebrafish Embryos. *Nat. Chem. Biol.* **2007**, *3* (10), 650–651. <https://doi.org/10.1038/nchembio.2007.30>.
- (58) Namiki, S.; Arai, T.; Fujimori, K. High-Performance Caged Nitric Oxide: A New Molecular Design, Synthesis, and Photochemical Reaction. *J. Am. Chem. Soc.* **1997**, *119* (16), 3840–3841. <https://doi.org/10.1021/ja962839d>.
- (59) Versaw, B. A.; Zeng, T.; Hu, X.; Robb, M. J. Harnessing the Power of Force: Development of Mechanophores for Molecular Release. *J. Am. Chem. Soc.* **2021**, *143* (51), 21461–21473. <https://doi.org/10.1021/jacs.1c11868>.
- (60) Chen, Y.; Mellot, G.; Van Luijk, D.; Creton, C.; Sijbesma, R. P. Mechanochemical Tools for Polymer Materials. *Chem. Soc. Rev.* **2021**, *50* (6), 4100–4140. <https://doi.org/10.1039/D0CS00940G>.

- (61) Fu, X.; Hu, X. Ultrasound-Controlled Prodrug Activation: Emerging Strategies in Polymer Mechanochemistry and Sonodynamic Therapy. *ACS Appl. Bio Mater.* **2024**, *7* (12), 8040–8058. <https://doi.org/10.1021/acsabm.4c00150>.
- (62) Martínez, R. F.; Cravotto, G.; Cintas, P. Organic Sonochemistry: A Chemist's Timely Perspective on Mechanisms and Reactivity. *J. Org. Chem.* **2021**, *86* (20), 13833–13856. <https://doi.org/10.1021/acs.joc.1c00805>.
- (63) Choi, V.; Rajora, M. A.; Zheng, G. Activating Drugs with Sound: Mechanisms Behind Sonodynamic Therapy and the Role of Nanomedicine. *Bioconjug. Chem.* **2020**, *31* (4), 967–989. <https://doi.org/10.1021/acs.bioconjchem.0c00029>.
- (64) Suslick, K. S. Sonochemistry. *Science* **1990**, *247* (4949), 1439–1445. <https://doi.org/10.1126/science.247.4949.1439>.
- (65) Mitragotri, S. Healing Sound: The Use of Ultrasound in Drug Delivery and Other Therapeutic Applications. *Nat. Rev. Drug Discov.* **2005**, *4* (3), 255–260. <https://doi.org/10.1038/nrd1662>.
- (66) Nyström, N. N.; Jin, Z.; Bennett, M. E.; Zhang, R.; Swift, M. B.; Shapiro, M. G. *Multiplexed Ultrasound Imaging of Gene Expression*; preprint; November 3, 2024. <https://doi.org/10.1101/2024.10.30.621148>.
- (67) Schrunk, E.; Dutka, P.; Hurt, R. C.; Wu, D.; Shapiro, M. G. Bioorthogonal Labeling Enables In Situ Fluorescence Imaging of Expressed Gas Vesicle Nanostructures. *Bioconjug. Chem.* **2024**, *35* (3), 333–339. <https://doi.org/10.1021/acs.bioconjchem.3c00518>.
- (68) Kosower, N. S.; Kosower, E. M.; Newton, G. L.; Ranney, H. M. Bimane Fluorescent Labels: Labeling of Normal Human Red Cells under Physiological Conditions. *Proc. Natl. Acad. Sci.* **1979**, *76* (7), 3382–3386. <https://doi.org/10.1073/pnas.76.7.3382>.
- (69) Liu, C. C.; Schultz, P. G. Adding New Chemistries to the Genetic Code. *Annu. Rev. Biochem.* **2010**, *79* (1), 413–444. <https://doi.org/10.1146/annurev.biochem.052308.105824>.
- (70) Birch-Price, Z.; Hardy, F. J.; Lister, T. M.; Kohn, A. R.; Green, A. P. Noncanonical Amino Acids in Biocatalysis. *Chem. Rev.* **2024**, *124* (14), 8740–8786. <https://doi.org/10.1021/acs.chemrev.4c00120>.

- (71) Hurt, R. C.; Jin, Z.; Soufi, M.; Wong, K. K.; Sawyer, D. P.; Shen, H. K.; Dutka, P.; Deshpande, R.; Zhang, R.; Mittelstein, D. R.; Shapiro, M. G. Directed Evolution of Acoustic Reporter Genes Using High-Throughput Acoustic Screening. *ACS Synth. Biol.* **2024**, *13* (7), 2215–2226. <https://doi.org/10.1021/acssynbio.4c00283>.
- (72) Lakshmanan, A.; Lu, G. J.; Farhadi, A.; Nety, S. P.; Kunth, M.; Lee-Gosselin, A.; Maresca, D.; Bourdeau, R. W.; Yin, M.; Yan, J.; Witte, C.; Malounda, D.; Foster, F. S.; Schröder, L.; Shapiro, M. G. Preparation of Biogenic Gas Vesicle Nanostructures for Use as Contrast Agents for Ultrasound and MRI. *Nat. Protoc.* **2017**, *12* (10), 2050–2080. <https://doi.org/10.1038/nprot.2017.081>.
- (73) Iskandar, S. E.; Haberman, V. A.; Bowers, A. A. Expanding the Chemical Diversity of Genetically Encoded Libraries. *ACS Comb. Sci.* **2020**, *22* (12), 712–733. <https://doi.org/10.1021/acscombsci.0c00179>.
- (74) Brouwer, B.; Della-Felice, F.; Illies, J. H.; Iglesias-Moncayo, E.; Roelfes, G.; Drienovská, I. Noncanonical Amino Acids: Bringing New-to-Nature Functionalities to Biocatalysis. *Chem. Rev.* **2024**, *124* (19), 10877–10923. <https://doi.org/10.1021/acs.chemrev.4c00136>.
- (75) Dieterich, D. C.; Link, A. J.; Graumann, J.; Tirrell, D. A.; Schuman, E. M. Selective Identification of Newly Synthesized Proteins in Mammalian Cells Using Bioorthogonal Noncanonical Amino Acid Tagging (BONCAT). *Proc. Natl. Acad. Sci.* **2006**, *103* (25), 9482–9487. <https://doi.org/10.1073/pnas.0601637103>.
- (76) Link, A. J.; Tirrell, D. A. Cell Surface Labeling of *Escherichia coli* via Copper(I)-Catalyzed [3+2] Cycloaddition. *J. Am. Chem. Soc.* **2003**, *125* (37), 11164–11165. <https://doi.org/10.1021/ja036765z>.
- (77) Ngo, J. T.; Tirrell, D. A. Noncanonical Amino Acids in the Interrogation of Cellular Protein Synthesis. *Acc. Chem. Res.* **2011**, *44* (9), 677–685. <https://doi.org/10.1021/ar200144y>.
- (78) Prescher, J. A.; Bertozzi, C. R. Chemistry in Living Systems. *Nat. Chem. Biol.* **2005**, *1* (1), 13–21. <https://doi.org/10.1038/nchembio0605-13>.

- (79) Van Hest, J. C. M.; Kiick, K. L.; Tirrell, D. A. Efficient Incorporation of Unsaturated Methionine Analogues into Proteins in Vivo. *J. Am. Chem. Soc.* **2000**, *122* (7), 1282–1288. <https://doi.org/10.1021/ja992749j>.
- (80) Li, J. C.; Nasertorabi, F.; Xuan, W.; Han, G. W.; Stevens, R. C.; Schultz, P. G. A Single Reactive Noncanonical Amino Acid Is Able to Dramatically Stabilize Protein Structure. *ACS Chem. Biol.* **2019**, *14* (6), 1150–1153. <https://doi.org/10.1021/acscchembio.9b00002>.
- (81) An, X.; Chen, C.; Wang, T.; Huang, A.; Zhang, D.; Han, M.; Wang, J. Genetic Incorporation of Selenotyrosine Significantly Improves Enzymatic Activity of *Agrobacterium Radiobacter* Phosphotriesterase. *ChemBioChem* **2021**, *22* (15), 2535–2539. <https://doi.org/10.1002/cbic.202000460>.
- (82) Chung, C. Z.; Krahn, N. The Selenocysteine Toolbox: A Guide to Studying the 21st Amino Acid. *Arch. Biochem. Biophys.* **2022**, *730*, 109421. <https://doi.org/10.1016/j.abb.2022.109421>.
- (83) Los, G. V.; Encell, L. P.; McDougall, M. G.; Hartzell, D. D.; Karassina, N.; Zimprich, C.; Wood, M. G.; Learish, R.; Ohana, R. F.; Urh, M.; Simpson, D.; Mendez, J.; Zimmerman, K.; Otto, P.; Vidugiris, G.; Zhu, J.; Darzins, A.; Klaubert, D. H.; Bulleit, R. F.; Wood, K. V. HaloTag: A Novel Protein Labeling Technology for Cell Imaging and Protein Analysis. *ACS Chem. Biol.* **2008**, *3* (6), 373–382. <https://doi.org/10.1021/cb800025k>.

